

ON THE BARYONIC, STELLAR, AND LUMINOUS SCALING RELATIONS OF DISK GALAXIES

V. AVILA-REESE¹, J. ZAVALA^{2,3}, C. FIRMANI^{4,1}, AND H. M. HERNÁNDEZ-TOLEDO¹

To appear in Astronomical Journal

ABSTRACT

We explore how the slopes and scatters of the scaling relations of disk galaxies (V_m - L [- M], R - L [- M], and V_m - R) do change when moving from B to K bands and to stellar and baryonic quantities. For our compiled sample of 76 normal, non-interacting high and low surface brightness (SB) disk galaxies, we find important changes, which evidence evolution effects, mainly related to the gas infall and star formation (SF) processes. We also explore correlations among the $(B - K)$ color, stellar mass fraction f_s , mass M (luminosity L), and surface density (SB), as well as correlations among the residuals of the scaling relations, and among these residuals and those of the other relations studied here. Some of our findings are: (i) the scale length R_{bar} is a third parameter in the baryonic Tully–Fisher relation (TFR) and the residuals of this relation follow a trend (slope ≈ -0.15) with the residuals of the R_{bar} - M_{bar} relation; for the stellar and K band cases, the scale length is not anymore a third parameter and the mentioned trend disappears; (ii) among the TFRs, the B -band TFR is the most scattered; in this case, the color is a third parameter, in agreement with previous works; (iii) the low SB galaxies break some observed trends in diagrams that include surface density, color, and f_s , suggesting then a threshold in the gas surface density Σ_g , below which the SF becomes independent of the gas infall rate and Σ_g . Our results are interpreted and discussed in the light of Λ Cold Dark Matter–based models of disk–galaxy formation and evolution. These models are able to explain not only the baryonic scaling correlations, but also most of the processes responsible for the observed changes in the slopes, scatters, and correlations among the residuals when changing to stellar and luminous quantities. The galaxy baryon fraction, f_{gal} , is required to be smaller than 0.05 on average. We detect some potential difficulties for the models: the observed color- M and surface density- M correlations are steeper, and the intrinsic scatter in the baryonic TFR is smaller than those predicted.

Subject headings: Cosmology: dark matter Galaxies: evolution – Galaxies: fundamental parameters – Galaxies: spiral – Galaxies: structure

1. INTRODUCTION

Disk galaxies are the main population of galaxies in the local Universe. The study of their global scaling relations is of paramount relevance for understanding the formation and evolution of galaxies in general. The main disk–galaxy observed global scaling relations are those between maximum circular velocity, V_m , and luminosity, L ; between disk scale length, R , and L ; and between V_m and R . Each one of these relations can be established for different optical/near-IR (NIR) pass-bands. Under some assumptions, analogous relations can be calculated for the corresponding stellar and baryonic quantities. The changes in the zero points, slopes and scatters of these relations, when changing from one color band to another, and to stellar and baryonic quantities, are expected to be intimately related to the stellar–population properties and radial distributions of disk galaxies. In turn, these properties and distributions depend mainly on the disk assembly and star–formation (hereafter SF) histories. Therefore, the study of the scale relations for different passbands and for the stellar and baryonic cases offers valuable information on the structural, dynamical

and SF properties of disk galaxies, as well as important constraints on models of their formation and evolution. The present paper is focused on this study.

1.1. Background on the disk scaling relations

The most robust and studied of the disk–galaxy scaling relations is the one between L and V_m , the so-called Tully–Fisher relation (TFR). Originally discovered in the B passband (Tully & Fisher 1977), it was afterward shown that it also applies to infrared bands. More recently, after applying a velocity (luminosity)–dependent extinction correction, Tully & Pierce (2000) have confirmed that the slope of the L - V_m correlation gets steeper systematically from B (≈ 2.9) to K (≈ 3.5) bands. This result suggests some dependence of galaxy colors on V_m for a given galaxy luminosity or mass. The amplitude of the scatter of the TFRs changes also with wavelength. These dependencies of the slope and scatter of the TFR on wavelength are related mainly to stellar population effects, which on their own, are related to the assembly and SF histories of galaxies. Regarding the intrinsic TFR scatters, they are found to be small, posing a challenge for scenarios aimed to explain the origin of disk galaxies (Eisenstein & Loeb 1996; Avila-Reese et al. 1998; Mo et al. 1998; Firmani & Avila-Reese 2000).

The TFR has widely been studied for estimating extragalactic distances. In this case the independent variable (predictor) is the circular velocity, and the galaxy samples are carefully pruned to minimize the scatter. The latter implies a selection of samples for a narrow range

¹ Instituto de Astronomía, Universidad Nacional Autónoma de México, A.P. 70-264, 04510 México D. F., México

² Instituto de Ciencias Nucleares, Universidad Nacional Autónoma de México, A.P. 70-543, 04510 México D.F., México.

³ Present affiliation: Shanghai Astronomical Observatory, Nandan Road 80, Shanghai 200030, China; jzavala@shao.ac.cn

⁴ INAF-Osservatorio Astronomico di Brera, via E.Bianchi 46, I-23807 Merate, Italy

of morphological types and surface brightnesses (hereafter SBs). However, for studies that aim to understand the origin of the TFR and use it to constrain models of galaxy formation rather than circular velocity, the luminosity should be the predictor, and the sample should be as wide as possible in morphological types, SBs, and colors (Courteau et al. 2007). Hereafter, we will refer to the TFR as the V_m - L (- M) correlation.

By using NIR magnitudes—which are good tracers of stellar masses—and gas contents when available, some authors have calculated the stellar and baryonic TFRs (e.g., McGaugh et al. 2000; Bell & de Jong 2001; Mayer & Moore 2004; Gurovich et al. 2004; Pizagno et al. 2005; de Rijcke et al. 2007). As discussed in Firmani & Avila-Reese (2000; hereafter FA-R), on one hand the baryonic TFR appears to be closely related to the cosmological halo maximum circular velocity–mass relation, and on the other hand, when compared to the stellar TFR, it reflects some aspects of the SF efficiency for different types of galaxies. The behavior of the scatter, when one changes from B - to K -band TFRs and to the stellar and baryonic TFRs, certainly contains relevant information on the processes of disk galaxy evolution such as gas infall, SF, and stellar population histories.

The radius for a given luminosity (or the disk SB) has been considered as a potential third parameter that correlates with the scatter of the TFR (e.g., Kodaira 1989; Willick 1999). The scale length R is indeed another structural parameter of disk galaxies that span a wide range of values. Some authors have reported that the scatter of the TFR is reduced up to 50% when R is introduced as a third parameter (e.g., Koda, Sofue & Wada 2000; Han et al. 2001). However, if the scatter of a given relation decreases upon introducing a third variable, it does not necessarily mean that such a variable is a statistically significant parameter. Indeed, some authors have shown that R (or central SB) is not a physical third parameter in the TFR (e.g., Han 1991; Tully & Verheijen 1997; Willick et al. 1997; Courteau & Rix 1999; FA-R), but the radius could be a third parameter in the baryonic TFR (FA-R; Avila-Reese, Firmani & Zavala 2002; Zavala 2003; Dutton et al. 2007).

It is well known that the radius correlate with L (Freeman 1970) and V_m (Tully & Fisher 1977), although these correlations are much more scattered than the TFR. Disk galaxies in the $\text{Log}L$ - $\text{Log}V_m$ - $\text{Log}R$ parameter-space indeed lie in a thin oblique plane whose edge-on projection is close to the $\text{Log}L$ - $\text{Log}V_m$ (TFR) projection (Koda, Sofue & Wada 2000; Han et al. 2001; Shen, Mo & Shu 2002; Gnedin et al. 2007). This is the so called fundamental plane of disk galaxies. Here we construct from observations and analyze separately each one of the three projections of these planes.

1.2. Construction and interpretation of the scaling relations: how do they change from luminous to stellar and baryonic quantities?

In most of the previous works, the disk-galaxy scaling correlations were constructed for samples biased in morphological types and SBs (pruned for reducing the scatter), and without selecting the environment. However, *for theoretical and interpretative studies, the observational galaxy sample should be as wide as possible in the range of morphologies, SBs, and colors* in order

to include the whole population of disk galaxies, later to be compared with model predictions. Besides, since galaxy models are commonly used for isolated galaxies, the observational sample should also be selected to contain galaxies *not affected by the environment*. On the other hand, the limited information of the samples employed in previous works, did not allow one to explore how the scaling correlations and their scatters change from luminous to stellar and baryonic quantities.

In this paper we shall use a sample of 76 disk galaxies compiled from the literature and homogenized in Zavala et al. (2003a; hereafter ZAHF) and Zavala (2003). This sample is not in any sense complete, an aspect that is crucial for volume-averaged population studies (e.g., the luminosity function), but is less relevant for studies on the correlations of physical properties. The sample includes high and low SB (hereafter HSB and LSB, respectively) disk *normal*⁵ galaxies of all morphological types, and it provides photometric information, at least in B and K bands, as well as information on the rotation curve and the HI integrated flux. None of the previous related works have presented a sample with these characteristics, which are crucial for the analysis proposed here. By using this sample, we will explore the differences in the slope and scatter of each scaling relation defined in the B and K bands, and for stellar and baryonic quantities. The results of this exploration will be interpreted in the light of disk-galaxy formation and evolution models.

The current theory of galaxy formation and evolution is based on the hierarchical Λ Cold Dark Matter (Λ CDM) cosmological model (for recent reviews, see Baugh 2006; Avila-Reese 2007). Several authors have attempted to predict the scaling relations of disk galaxies and their scatters within this model (e.g., Avila-Reese et al. 1998,2002; Mo et al. 1998; Steinmetz & Navarro 1999; Navarro & Steinmetz 2000; FA-R; Koda et al. 2000; Shen et al. 2002; Zavala 2003; Courteau et al. 2003,2007; Dutton et al. 2005,2007; Gnedin et al. 2007; Courteau et al. 2007). The results are encouraging. We shall use some of these results, mainly those of FA-R, to interpret and discuss the new inferences from observations presented here.

Note that it was a common practice in the literature to compare model results with the observed *luminous* properties and correlations, while most of the galaxy models did not actually include or self-consistently treat the process of gas transformation into stars, as well as did not follow the evolutionary path of halos and galaxies. As FA-R showed (see also Avila-Reese et al. 2002; Dutton et al. 2005), on one hand, there are systematical differences in the predicted scaling relations and their scatters among the luminous, stellar, and baryonic quantities; differences that we will explore here. On the other hand, properties such as the stellar and baryonic M , R , V_m , gas fraction, and integral colors depend not only on the initial parameters, but also on the evolutionary path of the halo-disk system (Stringer & Benson 2008). Contrary to the “static population” models, such as those of Mo et al. (1998) and extensions of them, the FA-R models are evolutionary. With some simplifications, they follow self-consistently (see Appendix B): the halo

⁵ Here we understand by normal galaxies: non-dwarf, non-interacting, nearly isolated local galaxies.

and disk assembly, taking into account the halo adiabatic contraction; the self-regulated disk SF and feedback; the luminosity evolution; and the secular bulge formation.

During the completion of the present work, several of the papers mentioned above, with results and a philosophy similar to ours, appeared in the literature. Although some overlapping is present, our contribution is original in the sense that we focus the research *on the changes in the scaling relations and their scatters when moving from optical to NIR bands and to stellar and baryonic quantities*. Our sample is similar in number to others used in recent works (e.g., Gnedin et al. 2007) and smaller with respect to Dutton et al. (2007) and Courteau et al. (2007), who use ~ 1300 objects with I -band photometry and $H\alpha$ kinematics, but only ~ 360 out of them, mainly HSB galaxies, have available K -band photometry. These large samples are undoubtedly useful and we will compare, when possible, with their results. However, we can not use them because they lack several observables (e.g., gas content, optical photometry) and requirements (e.g., inclination limits, LSB galaxies in both optical and K bands) that we have imposed for our study. We hope that our study will serve as a benchmark for similar analyzes based on large multiwavelength galaxy surveys, which are currently being completed.

This paper is organized as follows. In §2 we describe the disk galaxy sample to be used. The three main scaling correlations and their scatters are constructed and discussed in §3 for bands B and K and for the inferred stellar and baryonic quantities. Some other correlations among global galaxy quantities are also reported. In §4, in the light of previous Λ CDM-based disk galaxy formation and evolution models, we interpret the changes in the slopes and scatters of the scaling relations when changing from B to K bands and to stellar and baryonic quantities. A summary of the results and the conclusions of this work are presented in §6.

2. THE SAMPLE

In the literature there are only a few small galaxy samples with the requirements and data we need (broad in morphological types and SBs, with information on detailed surface-photometry in two separated pass-bands, e.g. B and K , on global dynamics, and on total HI gas flux). Here we use a compilation and completion of these samples presented in ZAHF and Zavala (2003; see also Graham 2002). In the following, we present the sub-samples, describe the homogenization and data correction processes that we have implemented, and the way in which we calculated the stellar and baryonic quantities (see ZAHF for additional details).

The sub-samples are: (i) de Jong & van der Kruit (1994; see also de Jong 1996a), which comprises undisturbed field, mostly HSB, disk galaxies, (ii) Verheijen (1997; see also Verheijen & Sancisi 2001), composed of disk HSB and LSB galaxies from the least massive and most spiral-rich nearby cluster, Ursa Minor, and (iii) Bell et al. (2000), a sample of LSB galaxies observed partially by them; the rest were compiled from the literature, mainly from de Blok et al. (1995,1996). In our sample we also included the Milky Way and Andromeda galaxies.

The raw photometric magnitudes, disk scale lengths, R , and central SBs were taken directly from the source

papers. In ZAHF and Zavala (2003) we have checked that there were no significant systematic differences in these parameters with inclination; we also found no systematics due to the different completeness criteria and profile fitting procedures used by the original authors of each sub-sample. In fact, the dominant source of error in the photometric parameters is caused by the uncertainty in the sky level (Bell et al 2000; de Jong 1996a). Regarding the dynamical information, and to make the data as uniform as possible, we used the velocity line-width W_{20} (defined at the 20% level) for almost all the galaxies in the sample. Only a few (LSB) galaxies in the sample lack a W_{20} measurement but have measured rotation curves; in these cases we have used the V_m inferred directly from the rotation curve. If properly corrected, $W_{20} \approx 2V_m$ (Verheijen 1997; Verheijen 2001). For the Verheijen sub-sample, we adopt the W_{20} values given in Verheijen & Sancisi (2001), while for the de Jong sub-sample and most of the LSB galaxies from the Bell et al. sub-sample, W_{20} was extracted from the HyperLEDA information system⁶. The integral fluxes in the 21-cm line (used to calculate the neutral gas mass component in galaxies) were taken from HyperLEDA, Verheijen & Sancisi (2001), and de Blok et al. (1996).

A condition imposed on our sample is that galaxies should be in a restricted range of inclinations ($35^\circ \leq i \leq 80^\circ$). We excluded from the sample any galaxies with clear signs of interaction (mainly from the Verheijen sub-sample) and with rotation curves that are still increasing at the last measured outer radius. Only some LSB galaxies showed this feature. The final sample consists of 76 galaxies: 42 out of 86, 29 out of 52, and 5 (8) out of 23 from the de Jong (1996a), Verheijen (1997), and Bell et al. (2000) sub-samples, respectively, plus the Milky Way and Andromeda galaxies. From the Bell et al. (2000) sample, 8 LSB galaxies are useful for us, but three of them are in common with the de Jong sample.

The local distances to the galaxies were calculated using the kinematic distance modulus given in HyperLEDA (see more details in ZAHF). The value of the Hubble constant used in this database is the same as that we assume here, $H_0 = 70 \text{ km s}^{-1} \text{ Mpc}^{-1}$. Since the LSB galaxies from the Bell et al. (2000) sub-sample are not included in HyperLEDA, their distances were taken directly from the source paper, properly corrected for the H_0 value used here.

The compiled sample is not complete in any sense, but it comprises representative ranges of the basic features of *normal* disk galaxies (see Fig. 1 in ZAHF). These features are mainly the morphological type, magnitude, disk central SB, integral color, and gas fraction.

2.1. Data corrections

The total magnitudes were corrected for Galactic extinction (following Schlegel et al. 1998), K term, and internal extinction (see ZAHF for details). For the latter we used the empirical velocity- (luminosity-) dependent extinction coefficients determined by Tully et al. (1998). The central SBs were corrected for Galactic extinction, K term, cosmological SB dimming, and inclination-geometrical and extinction effects- (see ZAHF). For the inclination correction, we followed Verheijen (1997),

⁶ <http://leda.univ-lyon1.fr>

considering LSB galaxies optically thin in all bands. The HSB galaxies were also considered optically thin in the K band. We have defined LSB galaxies as those with central SBs in the K band, after SB correction, larger than $18.5 \text{ mag/arcsec}^2$ (Verheijen 1997). The 21 cm line-widths at the 20% level, W_{20} , for the Verheijen subsample were taken directly from Verheijen & Sancisi (2001). Galaxies with W_{20} taken from LEDA were de-corrected (for instrumental corrections) to get the raw data (Paturel et al. 1997), and then corrected again for broadening due to turbulent motions and for inclination, this time following the procedure by Verheijen & Sancisi (2001).

In ZAHF, we did not take into account the observational errors. Here we attempt to estimate these errors for both the photometric and dynamic parameters, and use them for our results when possible. In Appendix A, we present our approach to estimate the errors.

2.2. Composite quantities

The stellar mass and disk central surface density, M_s and $\Sigma_{s,0}$, were derived from the K -band luminosity (which includes the bulge) and the extrapolated disk central SB, $\Sigma_{K,0}$, respectively, by using the appropriate stellar mass-to-light ratio, Υ_K . The application of population synthesis techniques to disk galaxy evolution models shows that Υ_K depends mainly on the integral color (Tinsley 1981; Bruzual 1983; Bell & de Jong 2001). In ZAHF we have used a Υ_K inferred from the latter paper. In a more recent work, Bell et al. (2003a) used galaxy evolution model fits for a large sample of galaxies from the Two Micron All Sky Survey (2MASS) and the Sloan Digital Sky Survey (SDSS). They obtained a correlation of Υ_K with $(B - R)$ color which is shallower and more scattered than that in Bell & de Jong (2001). Unfortunately, Bell et al. (2003a) did not report the correlation of Υ_K with the $(B - K)$ color. We have obtained this correlation by a re-scaling procedure that makes use of the Υ_K - $(B - R)$ correlation given in Bell et al. (2003a), and the Υ_K - $(B - R)$ and Υ_K - $(B - K)$ correlations given in Bell & de Jong (2001; their model “formation epoch with bursts” was used). We obtain the following result:

$$\text{Log}\Upsilon_K = -0.38 + 0.08(B - K). \quad (1)$$

For low SB values, at least for blue galaxies, Υ_K seems to anti-correlate with color (Verheijen 1997). In Fig. 1 of Bell & de Jong (2001), it is also shown how the inferred values of Υ_K , for low SBs, no longer decrease with decreasing SB, and even start to increase as SB decreases, although the scatter is large. In the absence of detailed models, we approximate the Υ_K - $(B - K)$ correlation for LSB galaxies in such a way that for $(B - K) > 3$, Υ_K is given by eq. (1), while for $(B - K) \leq 3$,

$$\Upsilon_K = 1.90 - 0.40(B - K). \quad (2)$$

The latter dependence is from a linear eye-fit to the Υ_K - $(B - K)$ correlation of the *blue* LSB galaxies in Verheijen (1997), for his case of a Hernquist halo model and the constrained decomposition method. After using the new Υ_K - $(B - K)$ correlations, the stellar and baryonic masses of the galaxy calculated here are slightly different from those used in ZAHF. The scale length of the stellar disk, R_s , is assumed to be equal to the scale length in the band K , R_K . Most of the stars in the disk are properly traced using this band.

The disk gas mass, M_g , is estimated as:

$$M_g = 1.4M_{\text{HI}} \left[1 + \frac{M_{\text{H}_2}}{M_{\text{HI}}} \right] \quad (3)$$

where the factor 1.4 takes into account helium and metals, and M_{H_2} is the mass in molecular hydrogen. The $M_{\text{H}_2}/M_{\text{HI}}$ ratio has been found to depend on the morphological type T (Young & Knesek 1989). Using the latter paper, McGaugh & de Blok (1997) estimated that $M_{\text{H}_2}/M_{\text{HI}} = 3.7 - 0.8T + 0.043T^2$. For $T < 2$, this empirical fitting formula could overestimate the gas mass in galaxies, thus we assume: $M_{\text{H}_2}/M_{\text{HI}} = 2.3$ (the value of the fit at $T = 2$) for $T < 2$.

The galaxy baryonic mass is defined as $M_{\text{bar}} = M_s + M_g$, and the gas mass fraction as $f_g = M_g/M_{\text{bar}}$. Unfortunately, we do not have information on the gas surface density profile parameters ($\Sigma_{g,0}$ and h_g) for the galaxies in our sample. We need them in order to calculate the baryonic disk central surface densities, $\Sigma_{\text{bar},0}$, and scale lengths, R_{bar} . As discussed in ZAHF, we assume that the total gas surface density follows an exponential distribution with a scale length 3 times that of R_K . Thus, $\Sigma_{g,0} = M_g/2\pi(3R_K)^2$. The baryonic quantity $\Sigma_{\text{bar},0}$ is then calculated as $\Sigma_{\text{bar},0} = \Sigma_{s,0} + \Sigma_{g,0}$. The corresponding baryonic radius will be then $R_{\text{bar}} = R_K[(\Sigma_{s,0} + 9\Sigma_{g,0})/\Sigma_{\text{bar},0}]^{0.5}$. In fact, the addition of the (uncertain) gas disk parameters will have little impact on our final results. This inclusion is important only for gas rich galaxies (late-type, blue LSB galaxies). We believe that in spite of the uncertainties, some real systematical variations of the baryonic disk scale length and surface density with the gas content of galaxies can still be taken into account through our procedure.

We have also estimated the errors in the composite quantities by adequately propagating the errors of the primary quantities. See Appendix A for details.

3. THE SCALING RELATIONS AND THEIR DISPERSIONS

For the sample of 76 galaxies presented in §2, we proceed to construct the physical scaling relations V_m - L ($-M$), R - L ($-M$), and V_m - R in the bands B and K , and for stars and baryons. Some authors recommend to use V_{flat} , the outer asymptotic flat part of the rotation curve, as an estimate of the circular velocity, instead of V_m . We stress that for studies aiming to understand the origin of the TFR and its scatter (the same applies for the V_m - R relation) as well as to compare them with galaxy model predictions, the adequate quantity to be used is V_m *because it maximizes the contribution of the disk component for a given halo*. By using V_{flat} , which traces the dynamics of the galaxy in outer regions, where the halo component tends to dominate, we lose information about the disk contribution. In fact, here we use neither V_m nor V_{flat} , but W_{20} . However, as mentioned in §2, there is some evidence that $W_{20} \approx 2V_m$.

For the luminosities and masses, here we use the total ones, i.e. the sum of disk and bulge. For the cases when bulges form by disk secular evolution processes (e.g. Avila-Reese & Firmani 2000; Avila-Reese et al. 2005), this is a good approximation for total disk luminosities and masses. For the scale length, the corresponding B and K band radii are used in the luminous scaling relations. For the stellar and baryonic scaling relations

we assume respectively $R_s=R_K$ and a scale length, R_{bar} , which takes into account the sum of the stellar and gas disks (see §2.2).

In Figs. 1–3, the observational points with the estimated error bars are plotted in the diagrams corresponding to the disk galaxy scaling relations studied here. The variables are given logarithmically. Circles and triangles are used for galaxies with $(B-K) > 3.0$ (red) and ≤ 3.0 (blue), respectively. The open and solid symbols are for galaxies with $\mu_{K,0} \leq 18.5$ (HSB) and $\mu_{K,0} > 18.5$ (LSB), respectively. To quantify the correlations and compare them among the different pass-bands and mass quantities (and eventually to model predictions), one needs to fit the correlations. To this end, a linear regression analysis should be used. We recall that our aim here is to explore variations for the scaling relations in the different cases (B and K bands, stars, and baryons) rather than study in detail the relations for each one of the cases. Therefore, it is important for us to *use the same regression method for all the cases rather than to choose an optimal method*.

For studies aimed at theoretical interpretations it is better to use a linear fit that is symmetric to interchanges of the two variables, e.g. the bisector or orthogonal regression linear methods. Here we fit the correlations using the forward, backward, bisector, and orthogonal linear regression models. However, for further analysis and discussion, *we will use only the orthogonal regression results*. The origin of coordinates for each correlation is shifted to the ‘barycenter’ of the corresponding variables, where the slope and zero point are uncorrelated.

The corresponding linear regressions, *not taking into account* the errors in the variables, were carried out for our galaxy sample in Zavala (2003) by using the SLOPES routine (Isobe et al. 1990; Feigelson & Babu 1992). This seems to be a feasible approximation when the intrinsic scatter in the regression line dominates any errors arising from the measurement and error propagation procedures (Isobe et al. 1990). The TFR is the tightest one among the scaling relations. Studies of the TFR have shown indeed that the intrinsic scatter of the linear fit is larger than the measurement and correction errors (for both magnitude and velocity). For example, Giovanelli et al. (1997) showed that the latter errors account for $\sim 0.25 - 0.15$ mag (from smaller to larger velocities), while the total scatter to the fit is $\sim 0.45 - 0.30$ mag for the same range of velocities, implying that the *intrinsic* scatter dominates over the measurement and correction uncertainties. For the other scaling relations, this difference is expected to be even larger.

Since we have obtained estimates of the errors in the variables of the scaling relations (Appendix A), here we carry out the corresponding ‘error-in-variable’ regression models. Thus, the analysis in the present paper is more exact than in Zavala (2003) and it allows us to roughly estimate the values of the intrinsic scatter in the different scaling relationships. Because the errors differ from point to point, the model should be heteroscedastic. We assume that the scaling relations have an (unknown) intrinsic scatter, which we want to estimate, explore, and confront with theory. The fitting regressions taking into account heteroscedastic measurement errors are carried out using the method and routine presented in Akritas & Bershady (1996). The total average intrinsic scatter,

TABLE 1
LINEAR DOUBLY-WEIGHTED FIT PARAMETERS AND SCATTERS
FOR THE TF (LOG-LOG) CORRELATIONS.

Fit	b	$\pm 1\sigma$	a	$\pm 1\sigma$	σ_{obs}	σ_{fit}	σ_{intr}
V_m-M_{bar}							
Forward	0.303	0.012	-0.979	0.127	0.029	0.058	0.050
Inverse	0.333	0.014	-1.300	0.151	0.031	0.063	0.055
Bisector	0.317	0.012	-1.140	0.132	0.030	0.060	0.052
Orthog.	0.306	0.012	-1.024	0.129	0.028	0.058	0.051
V_m-M_s							
Forward	0.274	0.011	-0.639	0.121	0.036	0.058	0.045
Inverse	0.294	0.013	-0.843	0.137	0.038	0.061	0.048
Bisector	0.284	0.012	-0.741	0.127	0.037	0.059	0.046
Orthog.	0.274	0.012	-0.650	0.123	0.035	0.058	0.045
V_m-L_K							
Forward	0.258	0.012	-0.503	0.126	0.014	0.052	0.050
Inverse	0.272	0.012	-0.652	0.132	0.015	0.057	0.054
Bisector	0.272	0.012	-0.652	0.132	0.014	0.054	0.052
Orthog.	0.261	0.012	-0.520	0.128	0.014	0.051	0.049
V_m-L_B							
Forward	0.310	0.015	-0.917	0.152	0.016	0.064	0.062
Inverse	0.361	0.016	-1.430	0.169	0.018	0.073	0.072
Bisector	0.335	0.014	-1.170	0.149	0.017	0.068	0.066
Orthog.	0.314	0.015	-0.963	0.154	0.016	0.065	0.063

NOTE. — $\text{Log}V_m = a + b\text{Log}M(L)$. V_m is given in kms^{-1} , M_{bar} and M_s in M_\odot , L_K in $L_{K\odot}$, and L_B in $L_{B\odot}$.

σ_{intr} , is estimated as the square root of the variance of the fit, σ_{fit}^2 , subtracted from the average (in both variables) observable variance, $\sigma_{\text{obs}}^2 (= N / \sum 1/[\sigma_y^2 + b^2\sigma_x^2])$, where N is the number of data points and b is the slope of the correlation), i.e., $\sigma_{\text{intr}}^2 = \sigma_{\text{fit}}^2 - \sigma_{\text{obs}}^2$. More elaborate fitting procedures could be used to estimate the intrinsic scatter (e.g., Gnedin et al. 2007). However, given the level of approximation we have used to determine the errors for the data, we consider that our first-order approximation is enough.

Tables 1–3 show the results from the different regression methods applied to the three scaling correlations in the four cases (baryonic and stellar quantities, and K and B bands). We report the zero point, a , the slope and b , with their respective standard deviations (calculated in the ‘barycenter’ of the variables), as well as the corresponding square roots of the variance of the fit, σ_{fit} , the bi-weighted average of the individual (in both variables) variances, σ_{obs} , and the total average intrinsic variance, σ_{intr} . We recall that our analysis, including the scatters, refers to the logarithm of the quantities involved. In the panels of Figs. 1 to 3, we plot the forward (dashed line), backward (dotted line), and orthogonal (solid line) doubly-weighted linear fits.

3.1. Luminosity (mass) vs velocity (TFRs)

As Fig. 1 and Table 1 show, the V_m-L_B , V_m-L_K , V_m-M_s and V_m-M_{bar} correlations are tight, although the differences between the lines obtained from the different regression methods are slightly larger than the dispersion associated with any given line. Therefore, the choice of the fitting method will slightly affect the results. For all the cases, the slopes of the forward correlations are shallower than those of the inverse correlations. For the bisector and orthogonal correlations, their slopes are between those of the forward and inverse correlations. The orthogonal correlations have shallower slopes than the bisector correlations, which are very close to those ob-

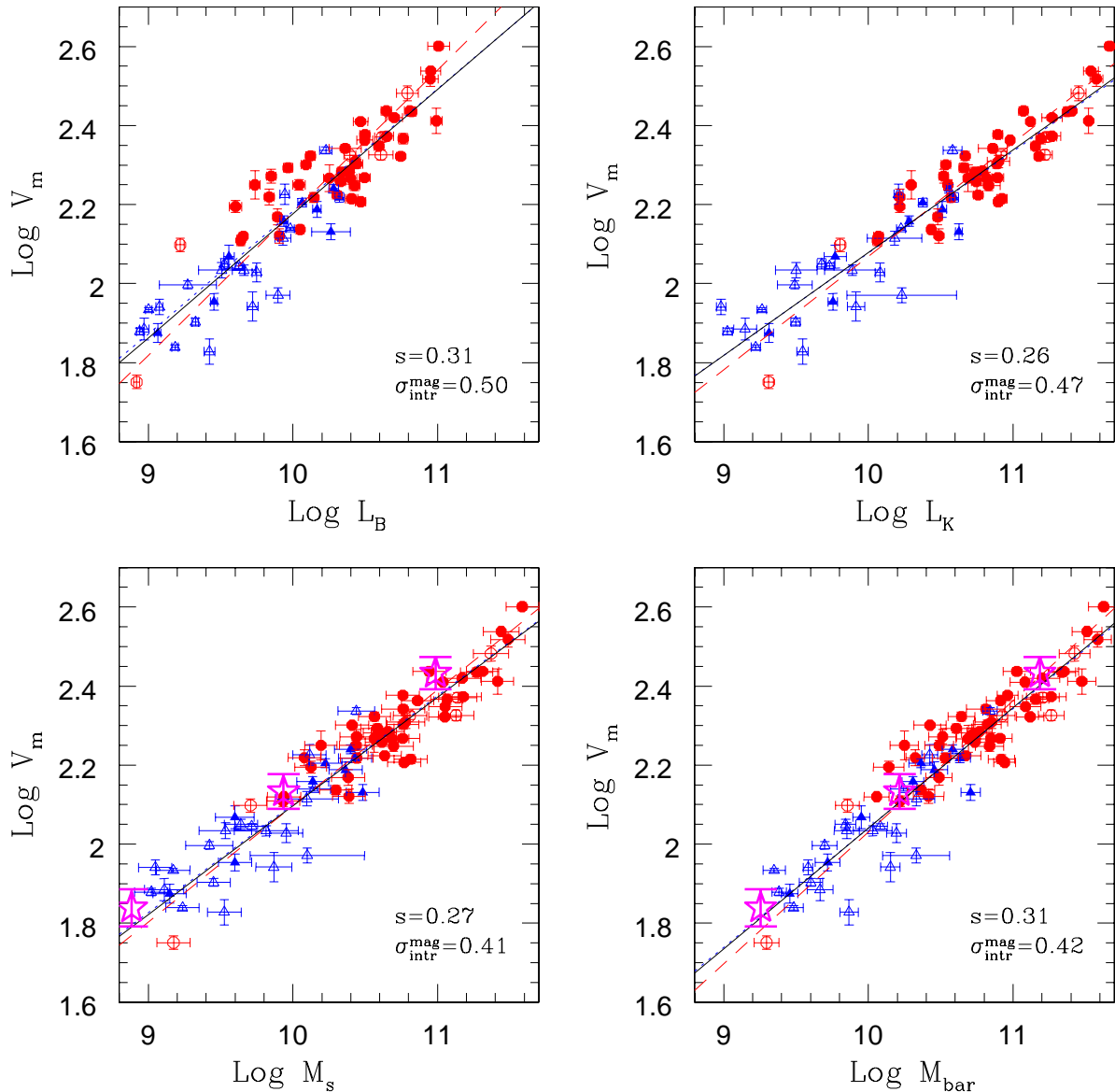


FIG. 1.— Observed TF correlations in the B and K bands (upper panels) and for stellar and baryonic masses (lower panels). V_m is in km/s and the luminosities and masses in the corresponding solar units. Solid and empty symbols are for HSB ($\mu_{K,0} \leq 18.5$ mag/arcsec²) and LSB ($\mu_{K,0} > 18.5$ mag/arcsec²) galaxies, respectively. Red galaxies ($[B - K] > 3$) are represented with (red) circles, while blue galaxies ($[B - K] \leq 3$) with (blue) triangles. The solid, dotted, and dashed lines are the corresponding orthogonal, forward, and inverse linear heteroscedastic doubly-weighted regressions, respectively. The slopes and inverse intrinsic scatters of the orthogonal fits are given inside each panel. The solid (magenta) stars with vertical error bars are the average values of V_m and the rms scatter for a given mass from the Λ CDM-based disk galaxy evolutionary models presented in FA-R ($\sigma_8 = 1$). The models were rescaled to $h = 0.7$.

tained from the forward fit. In the following, we analyze only the correlations fitted with the orthogonal regression method. A deep statistical analysis of each one of the correlations presented here is out of the scope of the paper.

From the baryonic V_m - M_{bar} to stellar V_m - M_s TFR, the slope is shallower by $\approx 11\%$, and the mass at $V_m = 160$ km/s is 1.36 times (0.134 dex) smaller; for larger velocities, the mass difference becomes smaller. From V_m - M_s to V_m - L_K , the slope remains almost constant. From V_m - L_K to V_m - L_B the slope is steeper by $\approx 20\%$, and some segregation by color appears.

Keeping in mind that most of the previous works used to report the forward slopes of the L -(M)- V_m correlations, we remark that the equivalent slopes here would

be the inverse of our inverse linear regressions (see Table 1): 3.00, 3.40, 3.67, and 2.77 for the baryonic, stellar, K - and B -band cases, respectively.

It should be noted that the sample used here is broad in galaxy properties and *it was not pruned to reduce the TFR scatter*. The few works that carry out analysis of samples similar to ours, although with different fitting methods, give slope values for the luminous TFRs (Kanappan, Fabricant & Franx 2002; Verheijen & Sancisi 2001; Dutton et al. 2007; Courteau et al. 2007) and for the stellar TFR (Pizagno et al. 2005; Gnedin et al. 2007) that are close to our estimates. The recent work by Pizagno et al. (2007), that analyzes a sample of 162 SDSS disk galaxies with $H\alpha$ rotation curves, reports slopes of the luminous TFRs that are much steeper than those

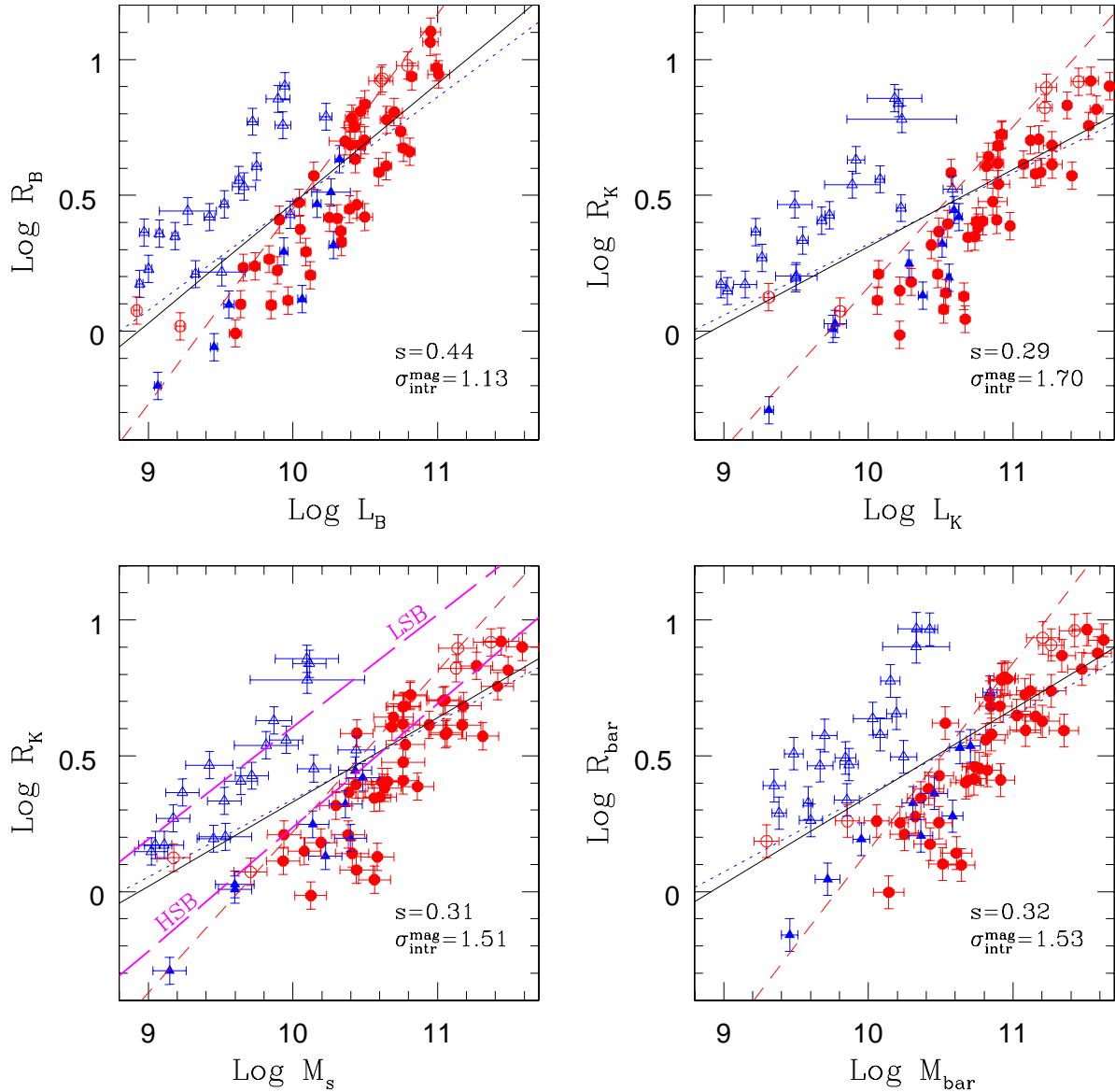


FIG. 2.— Observed radius–luminosity correlations in the B and K bands (upper panels), and radius–mass correlations for stellar and baryonic quantities (lower panels). Symbols, lines types, labels, and units are as in Fig. 1. Radii are in kpc. The thick dashed magenta lines in the R_K – M_s diagram are the fits to the model LSB and HSB+very HSB galaxies presented in FA-R (rescaled to $h = 0.7$).

obtained here. The baryonic TFR obtained in McGaugh (2005) is shallower than ours, however, he uses V_{flat} instead of V_m .

The estimated average intrinsic scatters, $\sigma_{\text{intr}}(\text{Log}V_m)$, in the V_m – M_{bar} , V_m – M_s , V_m – L_K , and V_m – L_B correlations are 0.051, 0.045, 0.049 and 0.063 dex, respectively. The intrinsic scatter is larger (by $\sim 10\%$) for the baryonic correlation than for the stellar one; the largest scatter is in the B –band. The intrinsic scatter along the M or L axis expressed in magnitudes, $\sigma_{\text{intr}}^{\text{mag}} = 2.5 \times \sigma_{\text{intr}}(\text{Log}V_m)/b$, oscillates between 0.41 mag (stellar correlation) and 0.5 mag (B band correlation) for all the regression methods used here (see values for the orthogonal fit in Fig. 1).

Recall that our observational error estimates and their propagation are approximations. Nonetheless, our estimates for the intrinsic scatter agree with other similar works. For example, Dutton et al. (2007) estimate $\sigma_{\text{intr}}(\text{Log}V_m) \approx 0.052$ in the I –band, which falls in between our values in the B and K bands. Pizagno et al.

(2007), who carried out a deep analysis of the errors for their sample, find typical values of the intrinsic scatter for the optical/NIR TFRs of 0.40–0.45 mag, which is close to our findings.

3.2. Radius vs luminosity (mass)

The R_B – L_B , R_K – L_K , R_s – M_s , and R_{bar} – M_{bar} correlations are scattered and strongly segregated by disk central SB (Fig. 2; Table 2). For a given luminosity or mass, the disk scale length, or central SB, span a large range of values. We see from Fig. 2 that a segregation by color is also present. There is no significant difference between the slopes and zero points of the baryonic and stellar R – M correlations. Both the mass and the radius increase when changing from stellar to baryon quantities, but the change is small and shifts galaxies along the same correlation, whose slope is ≈ 0.32 . From the stellar to the K –band correlation, the slope slightly decreases, while from the K – to the B –band correlation the slope

TABLE 2
LINEAR DOUBLY-WEIGHTED PARAMETERS AND SCATTERS FOR
THE RADIUS–MASS (LUMINOSITY) (LOG-LOG) RELATIONS

Fit	b	$\pm 1\sigma$	a	$\pm 1\sigma$	σ_{obs}	σ_{fit}	σ_{intr}
$R_{\text{bar}}-M_{\text{bar}}$							
Forward	0.287	0.035	-2.510	0.379	0.065	0.207	0.196
Inverse	0.692	0.098	-6.770	1.030	0.085	0.032	0.313
Bisector	0.474	0.042	-4.470	0.444	0.073	0.236	0.225
Orthog.	0.322	0.039	-2.870	0.422	0.067	0.208	0.197
$R_{\text{s}}-M_{\text{s}}$							
Forward	0.285	0.031	-2.510	0.327	0.061	0.196	0.187
Inverse	0.592	0.073	-5.700	0.765	0.087	0.282	0.269
Bisector	0.430	0.034	-4.020	0.366	0.072	0.218	0.206
Orthog.	0.310	0.033	-2.770	0.352	0.063	0.196	0.187
$R_{\text{K}}-L_{\text{K}}$							
Forward	0.262	0.030	-2.300	0.324	0.052	0.201	0.194
Inverse	0.593	0.075	-5.770	0.794	0.056	0.294	0.289
Bisector	0.418	0.035	-3.940	0.378	0.054	0.223	0.217
Orthog.	0.285	0.033	-2.540	0.355	0.052	0.201	0.194
$R_{\text{B}}-L_{\text{B}}$							
Forward	0.393	0.039	-3.460	0.403	0.053	0.206	0.198
Inverse	0.718	0.065	-6.730	0.658	0.058	0.278	0.271
Bisector	0.545	0.037	-4.980	0.387	0.055	0.223	0.216
Orthog.	0.441	0.044	-3.940	0.452	0.054	0.207	0.200

NOTE. — $\text{Log}R = a + b\text{Log}M(L)$. The radii are given in kpc, M_{bar} and M_{s} in M_{\odot} , L_{K} in $L_{\text{K}\odot}$, and L_{B} in $L_{\text{B}\odot}$.

TABLE 3
LINEAR DOUBLY-WEIGHTED REGRESSION PARAMETERS AND
SCATTERS FOR THE V_{m} -RADIUS (LOG-LOG) RELATIONS

Fit	b	$\pm 1\sigma$	a	$\pm 1\sigma$	σ_{obs}	σ_{fit}	σ_{intr}
$V_{\text{m}}-R_{\text{bar}}$							
Forward	0.332	0.078	2.030	0.044	0.024	0.160	0.158
Inverse	1.520	0.318	1.420	0.174	0.093	0.359	0.348
Bisector	0.768	0.056	1.810	0.044	0.048	0.201	0.195
Orthog.	0.506	0.109	1.937	0.063	0.033	0.167	0.164
$V_{\text{m}}-R_{\text{K}}$							
Forward	0.390	0.068	2.030	0.035	0.024	0.149	0.147
Inverse	1.220	0.196	1.670	0.096	0.063	0.274	0.267
Bisector	0.727	0.053	1.880	0.037	0.039	0.177	0.172
Orthog.	0.534	0.085	1.970	0.046	0.030	0.155	0.152
$V_{\text{m}}-R_{\text{B}}$							
Forward	0.378	0.057	2.010	0.035	0.023	0.142	0.140
Inverse	1.050	0.157	1.680	0.088	0.055	0.257	0.241
Bisector	0.662	0.049	1.870	0.038	0.036	0.167	0.163
Orthog.	0.481	0.067	1.960	0.043	0.028	0.146	0.143

NOTE. — $\text{Log}V_{\text{m}} = a + b\text{Log}R$. V_{m} is given in kms^{-1} , and the radii in kpc.

strongly increases, from 0.28 ± 0.03 to 0.44 ± 0.04 .

The intrinsic scatter measured in the Log of the radii is approximately the same in all the cases, $\sigma_{\text{intr}}(\text{Log}R) \approx 0.2$. When translated to the (X -axis) scatter in $\text{Log}L$ or $\text{Log}M$ and expressed in magnitudes, the scatter is around 1.1 mag for the B -band correlation and 1.5–1.7 mag for the other correlations. Hence, in the B band, the dispersion along the luminosity is decreased by some compensation effect. The observational errors in the R - L ($-M$) diagrams are significantly smaller than the corresponding average intrinsic scatters. Note that, contrary to the TFRs, for the R - L ($-M$) correlations, the use of a broad range in SBs (from HSB to LSB galaxies) significantly spreads the correlation and influences the slope and zero-point values. This can be clearly appreciated in Fig. 2: if we exclude the LSB galaxies, then the fit

changes notably. In most of the previous works aimed to estimate the disk scaling relations, *LSB galaxies were not considered. This is unfortunate if the observations are to be used to compare and constrain theoretical models.* Since the galaxy morphological type correlates with the SB, one expects that the R - L correlation also will depend on the type; Graham & Worley (2008) have indeed shown this explicitly.

3.3. Velocity vs radius

The $V_{\text{m}}-R_{\text{B}}$, $V_{\text{m}}-R_{\text{K}}$, and $V_{\text{m}}-R_{\text{bar}}$ correlations are shown in Fig. 3 and their fitting parameters are given in Table 3. The $V_{\text{m}}-R_{\text{s}}$ correlation is the same as the $V_{\text{m}}-R_{\text{K}}$ one because we assumed that $R_{\text{s}} = R_{\text{K}}$. The $V_{\text{m}}-R$ correlations are highly scattered, and segregated by disk surface brightness and color. For these correlations, the differences between forward and inverse fits are large. The relative errors in the fitted slope and zero point parameters are the largest ones among the three scaling relations studied here.

Because of the large dispersions in the fitted slopes and zero points of the $V_{\text{m}}-R$ correlations, there is no significant difference among these parameters when we change from the B to the K band and to the baryonic case. For the orthogonal regression, the slopes and zero points are ≈ 0.5 and ≈ 1.95 , respectively. The intrinsic scatter slightly decreases from the baryonic to the K -band, $\sigma_{\text{intr}}(\text{Log}V_{\text{m}}) \approx 0.17$ and 0.15, respectively. The estimated inverse intrinsic scatter (along the L axis) increases from the K to the B band.

3.4. Other global correlations

In order to complement the presented scaling correlations and their changes when moving from luminous to stellar and baryonic quantities, we explored the possibility of other correlations for our galaxy sample involving luminosities (masses), global color, central surface densities (brightnesses), and stellar mass content. Fig. 4 shows the $(B-K)$ color vs L_{B} , L_{K} , M_{s} , and M_{bar} , with the corresponding Pearson correlation coefficients and slopes. In spite of the L -dependent correction by internal extinction that we have applied, a clear correlation of color with L and M remains: more massive (luminous) galaxies are on average redder than the less massive (luminous) ones. The B -band correlation is the most scattered, as expected. The slope becomes slightly steeper when changing from M_{s} to M_{bar} mainly because the less massive, bluer galaxies have typically larger gas mass fractions, shifting more to the right side in the $\text{Log}M$ axis than the massive galaxies. The slope also becomes steeper when changing from L_{K} to L_{B} , in this case because less luminous galaxies being bluer on average, shift more to the right side in the $\text{Log}L$ axis than the redder luminous galaxies.

Noisy Log-Log correlations are also observed between $(B-K)$ and the different SBs and surface densities, and between the latter quantities and the luminosities and masses (Fig. 5). The slopes of the orthogonal fits are given inside each corresponding panel. The general trend is that the higher the surface density (or SB), the redder and more massive (luminous) is the galaxy. What lies on the basis of these trends for disk galaxies? We have also explored correlations related to the galaxy stellar's mass fraction, f_{s} (or gas mass fraction $f_{\text{g}} = 1 - f_{\text{s}}$). This

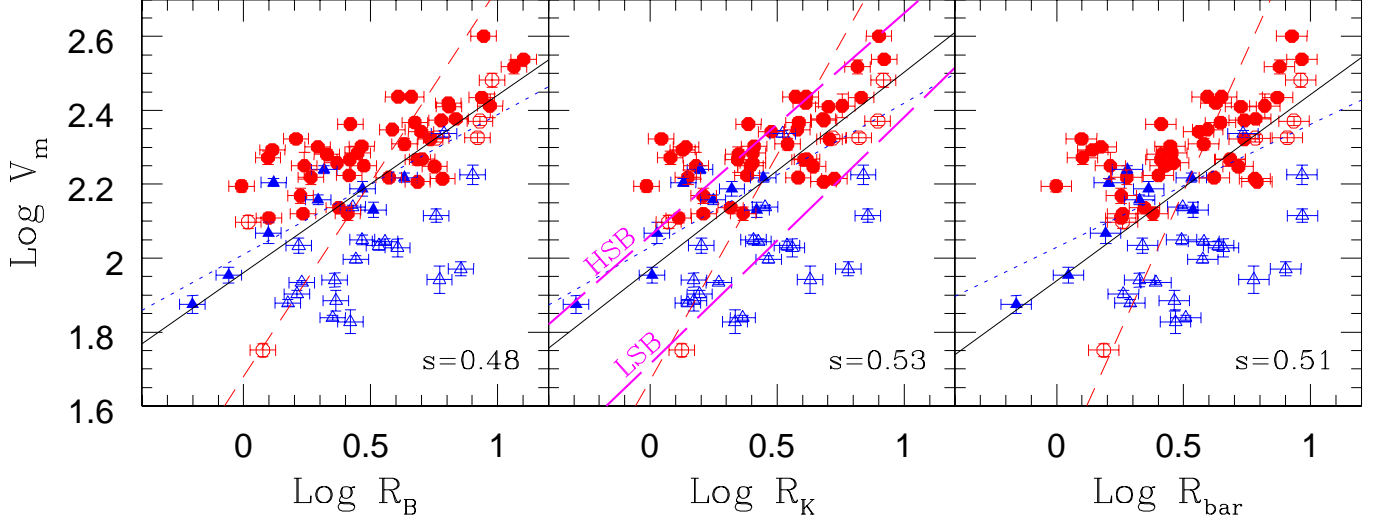


FIG. 3.— Observed V_m -radius correlations in the B and K bands (left and mid panels), and baryonic V_m - R_{bar} correlation (right panel). Because we assumed $R_s=R_K$, the stellar V_m - R_s correlation is as the V_m - R_K one. Symbols, line types and labels are as in Fig. 1. The thick dashed magenta lines are the fits to the model LSB and HSB+very HSB galaxies presented in FA-R (rescaled to $h=0.7$).

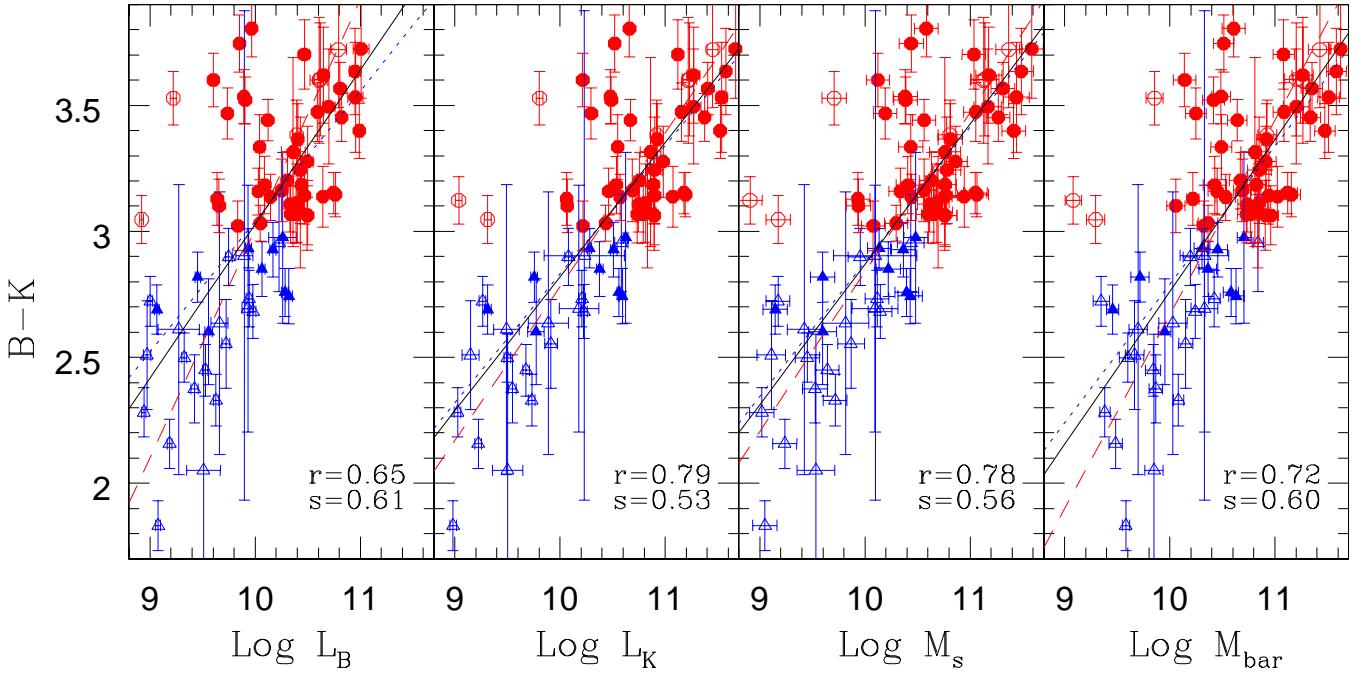


FIG. 4.— Corrected $(B-K)$ color vs the logarithms of L_B , L_K , M_s , and M_{bar} . Symbols and line types are as in Fig. 1. The Pearson's correlation coefficient, r , and the slope of the orthogonal fit, s , appear in the right-bottom corner of each panel.

quantity is an important property of galaxies related to their gas infall and SF rate histories; it will be discussed in §§4.2 (see Fig. 7 therein). The fraction f_s correlates strongly with the $(B-K)$ color and weakly with the surface densities (or SBs) and luminosities (masses), in that order. For all cases, the lowest SB galaxies break the correlations, suggesting a kind of a threshold for the gas surface density, below which the SF efficiency is almost independent of it (and of M or L).

3.5. Residual correlations and the search for other significant parameters in the scaling relations

To gain a more quantitative description of the disk galaxy scaling relations and their implications, we may explore the behavior of their residuals. The possible correlations of the residuals among them, and other galaxy properties, bring valuable information on galaxy formation and evolution processes. In particular, the changes of the residual correlations when moving from optical to NIR bands and to stellar and baryonic quantities provide clues on the SF and stellar population evolution processes as well as on the dynamics of disk galaxies.

In the different panels of Fig. 6, the residuals of the V_m - $M(-L)$ correlations are plotted against the corresponding residuals of the R - $M(-L)$, $(B-K)$ - $M(-L)$, and f_s - $M(-L)$

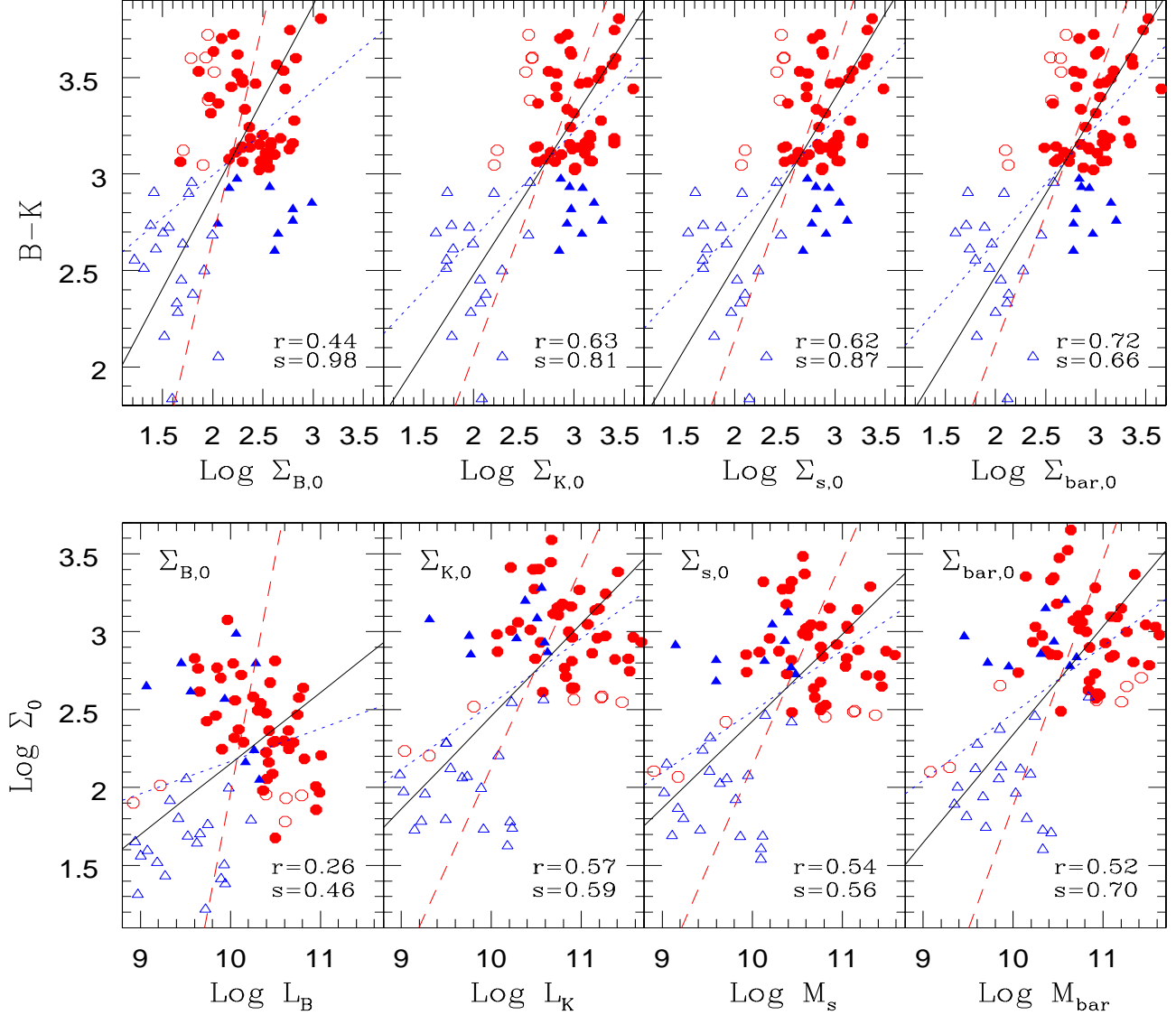


FIG. 5.— Corrected $(B - K)$ color vs the Log of $\Sigma_{B,0}$, $\Sigma_{K,0}$, $\Sigma_{s,0}$ and $\Sigma_{\text{bar},0}$ (top panels), and $\text{Log } \Sigma_0$ vs $\text{Log}(M, L)$ for B, K bands, stellar and baryonic components from left to right (bottom panels). Symbols and line types are as in Fig. 1. Labels are as in Fig. 4.

correlations for the baryonic, stellar, K - and B -band cases, respectively. The orthogonal regression fit was used to obtain the residuals. As can be seen in Fig. 6, for most of the cases, the residuals are weakly correlated or completely uncorrelated with each other.

For the baryonic case, we find an anti-correlation of $\Delta V_m(M_{\text{bar}})$ with $\Delta R_{\text{bar}}(M_{\text{bar}})$ with a slope of -0.15 ± 0.04 (orthogonal linear regression): on average, the more a galaxy deviates in the direction of the high-velocity side in the V_m - M_{bar} relation, then the more it deviates in the direction of the small-radius side in the R_{bar} - M_{bar} relation. It is illustrative to know that for the extreme case of exponential disks without dark matter halos, the slope would be -0.5 , while for completely halo dominated galaxies, no correlation is expected. For the stellar and K - and B -band cases, the trend described above almost disappears. These results show that *the residuals of the V_m - L ($-M$) and R - L ($-M$) correlations can or cannot correlate, depending not only on the inner*

dynamics of the galaxies themselves, but also on their SF histories, a question highlighted in FA-R. From the left column of Fig. 6, we also learn that for all cases, the LSB galaxies are more scattered and uncorrelated than the HSB ones in the residuals plane.

As expected, the residuals of the R - L ($-M$) correlations anti-correlate strongly with the corresponding disk central surface densities (or SBs) as: $\Delta R_{\text{bar}}(M_{\text{bar}}) \propto \Sigma_{\text{bar},0}^{-0.34}$, $\Delta R_s(M_s) \propto \Sigma_{s,0}^{-0.39}$, $\Delta R_K(L_K) \propto \Sigma_{K,0}^{-0.37}$, and $\Delta R_B(L_B) \propto \Sigma_{B,0}^{-0.45}$. The surface density (or SB) is clearly a significant third parameter in all the R - L ($-M$) correlations. The tightest anti-correlation is for the baryonic case; then its strength decreases successively for the stellar, K -band, and B -band cases. The residuals of the V_m - R correlations correlate significantly with the corresponding surface densities (or SBs). These residuals also correlate with those of the V_m - L ($-M$) correlations, but with a considerable segregation by SB (or surface density), resembling the R - L ($-M$) correlations.

The findings reported above imply that the radius could be a statistically significant third parameter in the baryonic TFR. Applying a backward step-wise multiple linear regression procedure, where F tests are used to compute the significance of each independent variable⁷, Zavala (2003) has indeed found that the radius is a third (statistically significant) parameter in the baryonic TFR. However, the radius was no longer found to be a third parameter in the stellar and luminous TFRs. We confirm here the results by Zavala (2003), with the exception that for our analysis in the B band, the radius is statistically more significant than in the analysis of Zavala (2003), however, we still find that the radius is not a third parameter in the B -band TFR; instead, the $(B-K)$ color is a third parameter in this case.

Since we are interested in the changes in the scaling correlations when changing from one band to another and to stellar and baryonic quantities, it is important then to analyze also the possible dependences of their residuals on galaxy color and stellar fraction. In the mid and right panels of Fig. 6, the residuals of the V_m - L ($-M$) correlations are plotted vs the residuals of the $(B-K)$ - L ($-M$) and f_s - L ($-M$) correlations, rather than just vs $(B-K)$ and f_s . In this way, the comparisons are at a given L or M . In the baryonic case, there are noisy trends: the residuals of the V_m - M_{bar} correlation increase on average for increasing residuals of the $(B-K)$ - M_{bar} and f_s - M_{bar} correlations (the galaxies become redder and with higher f_s); however, this is only true for the HSB galaxies. In the stellar and K -band cases, one does not see any clear trend. In the B band, the residuals $\Delta V_m(L_B)$ correlate with the residuals $\Delta(B-K)(L_B)$, although mainly due to the HSB galaxies. The backward step-wise analysis shows that the $(B-K)$ color is indeed the third parameter in the B -band TFR (see also Kannappan et al. 2002; Pizagno et al. 2007; Courteau et al. 2007). There is also a weak correlation of $\Delta V_m(L_B)$ with $\Delta f_s(L_B)$.

4. INTERPRETING THE SCALING RELATIONS

The results reported in §3 reveal non-negligible changes in the slopes and scatters of the scaling correlations of disk galaxies when changing from B to K bands and to stellar and baryonic quantities. While the most robust aspects of the scaling relations seem to be a consequence of the cosmological initial conditions of disk galaxy formation (e.g., FA-R; Shen et al. 2002; Dutton et al. 2007), the changes found here are expected to be related mainly with the SF and gas infall histories of galaxies. In the following, we focus our discussion on the findings presented in §3 and on whether or not these changes are expected in Λ CDM-based models of disk galaxy evolution.

4.1. The baryonic relations

The scenario of disk galaxy formation sketched in Appendix B makes certain predictions regarding the bary-

onic scaling relations of disk galaxies (Appendix C). The main simple physical ingredients of disk galaxy formation and evolution are the halo mass M_h , the mass assembly history (MAH), the spin parameter λ , and the disk galaxy mass fraction $f_{\text{gal}} \equiv M_{\text{bar}}/M_h$. Below, we highlight some of the main aspects of these predictions with the goal of interpreting the observational inferences presented in §3. At some points, we will discuss in more detail the model results obtained in FA-R. In that work, the cosmology used corresponded to a flat Λ CDM universe with $\Omega_{M,0} = 0.35$, $\Omega_\Lambda = 0.65$, $h = 0.65$, $\sigma_8 = 1$; f_{gal} was assumed to be constant.

The V_m - M_{bar} relation. As described in Appendix C1, if the initial condition parameters λ and f_{gal} do not depend significantly on mass, then one expects that the baryonic TFR should have a slope similar to the cosmological one. *This seems to be the case according to our results* ($a_{\text{bar}} \approx 0.31$ from observation vs $a_{\text{halo}} = 0.30 - 0.32$ from simulations). The models of FA-R and Dutton et al. (2007) show that for a reasonable range of f_{gal} values (between $\sim 0.03 - 0.08$), changes of f_{gal} with mass would not have a significant effect on the baryonic TFR slope (taking into account the disk gravitational drag on the halo); for a given M_h , as f_{gal} decreases, M_{bar} decreases, but V_m also decreases (actually is the G function defined in the Appendix C1 that decreases), and the galaxy model shifts along the relation. In the same way, a moderate correlation (anti-correlation) of λ with mass would only slightly decrease (increase) the slope. Conversely, steep dependences of f_{gal} and/or λ upon mass would imply a significant change in the slope of the TFR.

Regarding the intrinsic scatter, we have measured from the observational sample a value of $\sigma_{\text{intr}}(\text{Log}V_m) = 0.051$ for the baryonic TFR. This value, in spite of the broadness of the sample, *is in marginal agreement with the theoretical expectations discussed in Appendix C1*. For example, for the FA-R models with $f_{\text{gal}} = 0.05$, $\sigma_{\text{intr}}(\text{Log}V_m) \approx 0.053$; by relaxing some model assumptions, this value is expected to be larger. Thus, from the comparison of observations with theory, it seems that there is no room for other significant sources of scatter, either physical or systematical, as for example disk ellipticity and non-circular motions (see §5 for further discussion).

Further pieces of information related to the scatter in the baryonic TFR are given by the correlations between the residuals of this relation, $\Delta V_m(M_{\text{bar}})$, and those of the R_{bar} - M_{bar} , $(B-K)$ - M_{bar} and f_s - M_{bar} correlations (Fig. 6). The fact that $\Delta V_m(M_{\text{bar}})$ anti-correlates with $\Delta R_{\text{bar}}(M_{\text{bar}})$ shows that *the radius (or surface density) plays a role in the scatter of the baryonic TFR*. As mentioned in §3.5, the radius is found to be indeed a statistically significant parameter in the V_m - M_{bar} - R_{bar} multi-variable correlation. Because $\Delta R_{\text{bar}}(M_{\text{bar}})$ correlates strongly with $\Sigma_{\text{bar},0}$ (§3.5), the anti-correlation seen in Fig. 6 implies that, for a given M_{bar} , higher surface density disks produce larger values of V_m . For a given λ distribution, the larger f_{gal} , the higher the disk surface density, and hence the more pronounced is the effect upon V_m because the disk contribution to the total rotation curve is larger. This implies a steeper and stronger anti-correlation between $\Delta V_m(M_{\text{bar}})$ and $\Delta R_{\text{bar}}(M_{\text{bar}})$. In the extreme case of complete dominion of an exponential disks (no dark matter halo), this anti-correlation

⁷ In this analysis, V_m is assumed to be the dependent variable and M (or L), Σ_0 , R , $(B-K)$, f_g , and the morphological type T are the independent variables. For each case (baryonic, stellar, and B and K bands), one starts from a multiple variable linear regression using *all* the variables and then, through the backward step-wise procedure, the variables that are not statistically significant are eliminated step by step.

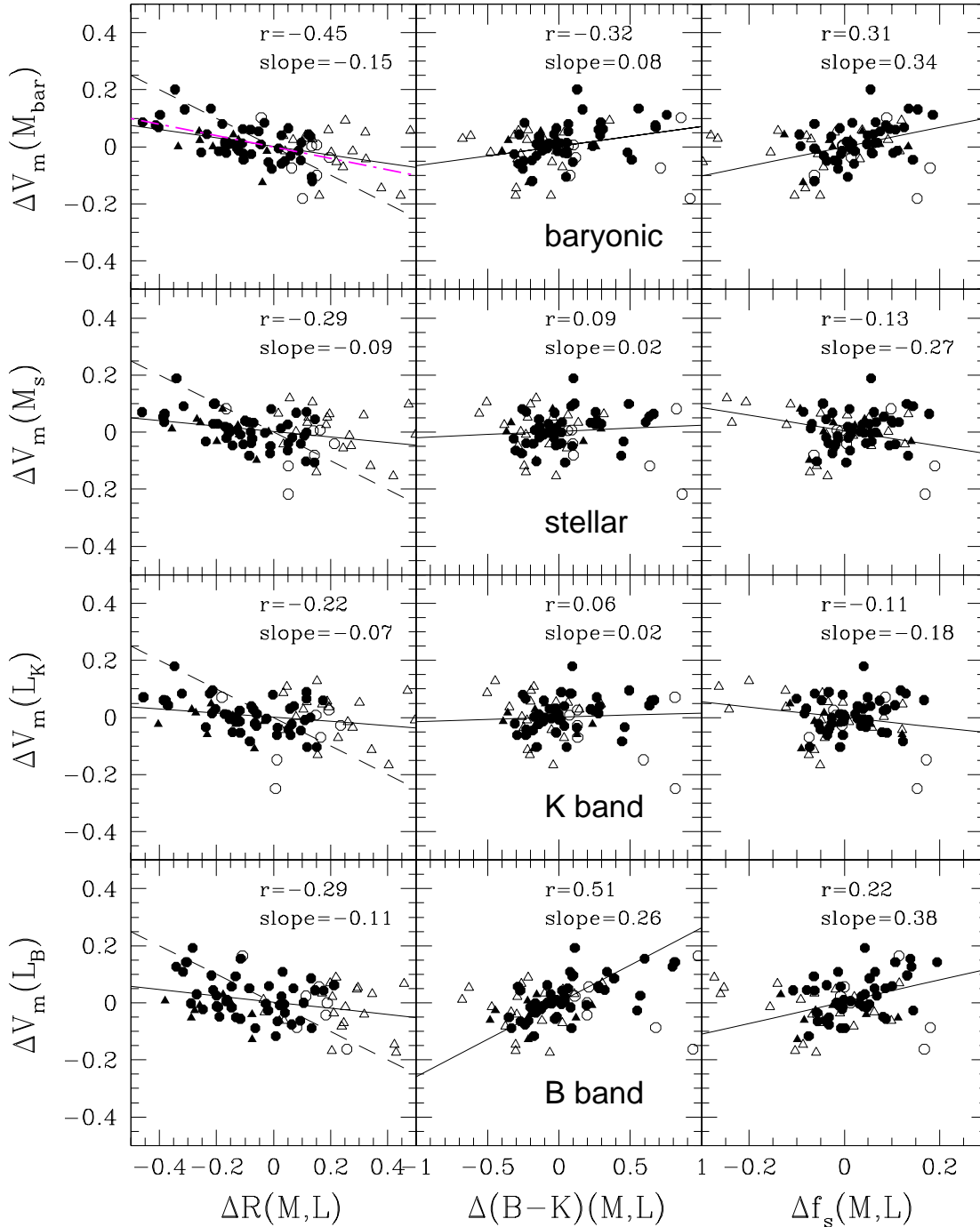


FIG. 6.— Residuals of the different TF correlations vs the residuals of the different radius–mass (luminosity), color–mass (luminosity), and f_s –mass (luminosity) correlations. From top to bottom, the rows correspond to the baryonic, stellar, K and B band cases. Symbols are as in Fig. 1. The solid lines are the orthogonal linear regressions. The corresponding Pearson correlation coefficients and the slopes are given inside each panel. The dot–dashed (magenta) line in the upper left panel is the linear fit to the model results by FA-R. The dashed lines in all the panels in the left column indicate the prediction for an exponential disk without dark halo (slope -0.5).

should have a slope of -0.5 (Courteau & Rix 1999).

Our observational results point to a slope shallower than -0.5 , ≈ -0.15 , showing that the dark halo contribution at a radius where the rotational velocity is maximal, is significant, as predicted by models based on Λ CDM halos. According to Fig. 6, the residuals are more tightly anti-correlated for the HSB sub-sample than for the LSB sample. This implies that the dark halo component becomes more dominant for lower values of the disk SB, to the point that the contribution of the disk to the total rotation curve at radii close to its maximum,

is negligible for the lowest SB galaxies. This dependence of the baryon and dark matter contents with SB has been deeply explored in ZAHF, who showed that for the same galaxy sample used here, only the highest SB disk galaxies are maximum disk, while the lower the SB, the more dark-halo-dominated (sub-maximum disk) the galaxies become (see also e.g., Casertano & van Gorkom 1991; de Blok & Bosma 2002; Catinella et al. 2007). It is important to mention that the slope of the residual correlation is sensitive to f_{gal} . For the modeling of disks formed inside Λ CDM halos discussed above, the slope will be

significantly steeper than -0.15 if the average value of f_{gal} is larger than 0.05 (e.g., Gnedin et al. 2007; Dutton et al. 2007; Pizagno et al. 2007). For the cosmology used by FA-R and $f_{\text{gal}}=0.05$, they found that the slope is ≈ -0.20 (see their Fig. 8). An interesting question is *what slope would be predicted by alternative theories, like the Modified Newtonian Dynamics, and would agree with the value of ≈ -0.15 found here using a broad sample of disk galaxies.*

We stress that observational studies aimed to constrain the baryon and dark matter contents in disk galaxies should use the baryonic relations instead of the luminous or stellar ones. For example Courteau & Rix (1999) obtained the residuals of the observed (infrared) TFR and R - L relation for a sample of mostly HSB galaxies, and interpreted the lack of correlation between these residuals as evidence of dark matter dominance in all galaxies. As FA-R showed, the dependency among the residuals changes from the baryonic to the stellar relations (see also Dutton et al. 2007; Courteau et al. 2007). Our observational results confirm this fine effect.

The $R_{\text{bar}}-M_{\text{bar}}$ relation. For the galaxy sample analyzed here, the $R_{\text{bar}}-M_{\text{bar}}$ correlation is highly scattered ($\sigma_{\text{intr}}(\text{LogR})=0.2$ for the orthogonal fit), with the scatter indeed anti-correlating strongly with $\Sigma_{\text{bar},0}$ ($r = -0.91$), and less with the $(B - K)$ color, as the Λ CDM-based models predict (Appendix C2). The slope of the correlation, for the orthogonal fit, is 0.32 ± 0.04 (Table 2) and is steeper for the bisector and inverse fits, i.e. is close to the slope of the CDM halo $R_{\text{h}}-M_{\text{h}}$ relation (Appendix B). *Thus, according to the arguments given in Appendix C2, there is almost no room for a significant dependence of λ or f_{gal} on M_{bar} , in the range of masses of the galaxies studied here, although if both parameters anti-correlate (or correlate) at the same time with M_{bar} then the slope changes may be compensated.*

The $V_{\text{m}}-R_{\text{bar}}$ relation. The slope of the (noisy) $V_{\text{m}}-R_{\text{bar}}$ correlation found here is 0.51 ± 0.11 (orthogonal fit), i.e. shallower than the cosmological one (see Appendix B). This, according to Appendix C3 *favours, if any, an anti-correlation of f_{gal} with mass.* The intrinsic scatter, $\sigma_{\text{intr}}(\text{Log}V_{\text{m}})=0.16$, is much larger than the scatter around the baryonic TFR. As predicted by the models, the residuals of the $V_{\text{m}}-R_{\text{bar}}$ correlation correlate significantly with both $\log\Sigma_{\text{bar},0}$ and the $(B - K)$ color ($r = 0.95$ and 0.67 , respectively); the slopes of these correlations (orthogonal fit) are 0.34 and 0.28 , respectively.

4.2. The stellar relations

The main changes when moving from the baryonic to the stellar scaling correlations are the decrease of the slope and intrinsic scatter in the $V_{\text{m}}-M$ correlations. The scatters of the $R-M$ and $R-V_{\text{m}}$ correlations also decrease but the significance of these decrements are very marginal. More interestingly, the (weak) anti-correlation between the residuals of the baryonic $V_{\text{m}}-M_{\text{bar}}$ and $R_{\text{bar}}-M_{\text{bar}}$ correlations tends to disappear in the stellar case. This is a fact related to other of our results, namely that *the radius (or disk surface density) is a third parameter in the baryonic TFR but no longer in the stellar one.* All these differences are related to the gas (or stellar) mass fraction of galaxies, and they show that the mass infall and SF histories vary systematically among galaxies. Are these variations consistent with galaxy models based on

the Λ CDM framework?

Let us first discuss the change in the slope of the $V_{\text{m}}-M$ relation. If the stellar mass fraction, $f_{\text{s}} = 1 - f_{\text{g}}$, depends on M_{s} as $f_{\text{s}} \propto M_{\text{s}}^{\beta}$, then $M_{\text{bar}} = M_{\text{s}}/f_{\text{s}} \propto M_{\text{s}}^{1-\beta}$. Therefore, from $V_{\text{m}} \propto M_{\text{bar}}^{\alpha}$ one passes to $V_{\text{m}} \propto M_{\text{s}}^{\alpha(1-\beta)}$. In the left panel of Fig. 7, we show f_{s} vs M_{s} for our galaxy sample. Although with a high scatter, f_{s} correlates with M_{s} roughly as

$$f_{\text{s}} = 0.65(M_{\text{s}}/10^{10}M_{\odot})^{0.13}, \quad (4)$$

implying then that the slope from the baryonic to stellar TFRs should decrease by a factor ~ 0.87 . The corresponding slopes calculated with the orthogonal fits are 0.31 and 0.27 , respectively. What causes the dependence of f_{s} (or f_{g}) on M_{s} ? It could be that rather than a fundamental dependence, it is a consequence of other correlations. For example, Fig. 7 shows that f_{s} correlates stronger with $\Sigma_{\text{s},0}$ (and also with galaxy color) than with M_{s} .

From the point of view of the models, the stellar fraction f_{s} of normal disk galaxies depends mainly on two factors: the efficiency of gas transformation into stars, given basically by the disk surface density (determined by λ , f_{gal} , and M_{h}), and the gas infall history, connected to the halo MAH. Based on these processes and by means of semi-numerical models, FA-R and Avila-Reese & Firmani (2000) have shown that (i) lower surface density disks transform gas into stars with less efficiency than disks of high surface density, (ii) more massive disks tend to be of higher surface density (see also Dalcanton et al. 1997), and (iii) the present-day f_{s} correlates significantly with $\Sigma_{\text{s},0}$ (or $\Sigma_{\text{B},0}$), and because of item (ii), with M_{s} . Note that the dependence of f_{s} on $\Sigma_{\text{s},0}$ is a non trivial prediction because several physical/evolutionary processes combine to give rise to the stellar (or gas) mass fraction and surface density (brightness) of evolved disk galaxies. In Fig. 7, together with the observational inferences, the model predictions presented in FA-R are plotted in the $f_{\text{s}}-\Sigma_{\text{s},0}$ diagram (magenta stars). Models and observations occupy the same region, though the models have on average slightly lower f_{s} and $\Sigma_{\text{s},0}$ values; the introduction of interaction-driven SF would work in the direction of increasing both quantities.

As a consequence of the mentioned predictions, FA-R showed that the scatter around the stellar TFR due to λ ($\Sigma_{\text{bar},0}$) should diminish compared to the one around the baryonic TFR; from the baryonic to the stellar TFR, the average scatter decreases from $\sigma_{\text{intr}}(\text{Log}V_{\text{m}}) \approx 0.053$ to $\sigma_{\text{intr}}(\text{Log}V_{\text{m}}) \approx 0.040$. Galaxies that in the baryonic TFR were shifted to the high- V_{m} side, because of their higher surface densities, transform gas into stars more efficiently and shift also to larger M_{s} values in the stellar TFR diagram compared to galaxies of lower surface densities. As a result, the dispersion in the stellar TFR due to disk surface density (mainly associated to λ and f_{gal}) decreases, and *the TFR becomes almost the same for HSB and LSB galaxies: the anti-correlation between the residuals of the TFR and those of the $R_{\text{s}}-M_{\text{s}}$ relation disappears.* The dispersion in the halo MAH remains as the main source of scatter in the stellar TFR. However, regarding the original MAH dispersion, it is also predicted that there is a kind of compensation in the shift of galaxies in the $V_{\text{m}}-M$ diagrams: galaxies that were shifted to the high- V_{m} side because they were formed

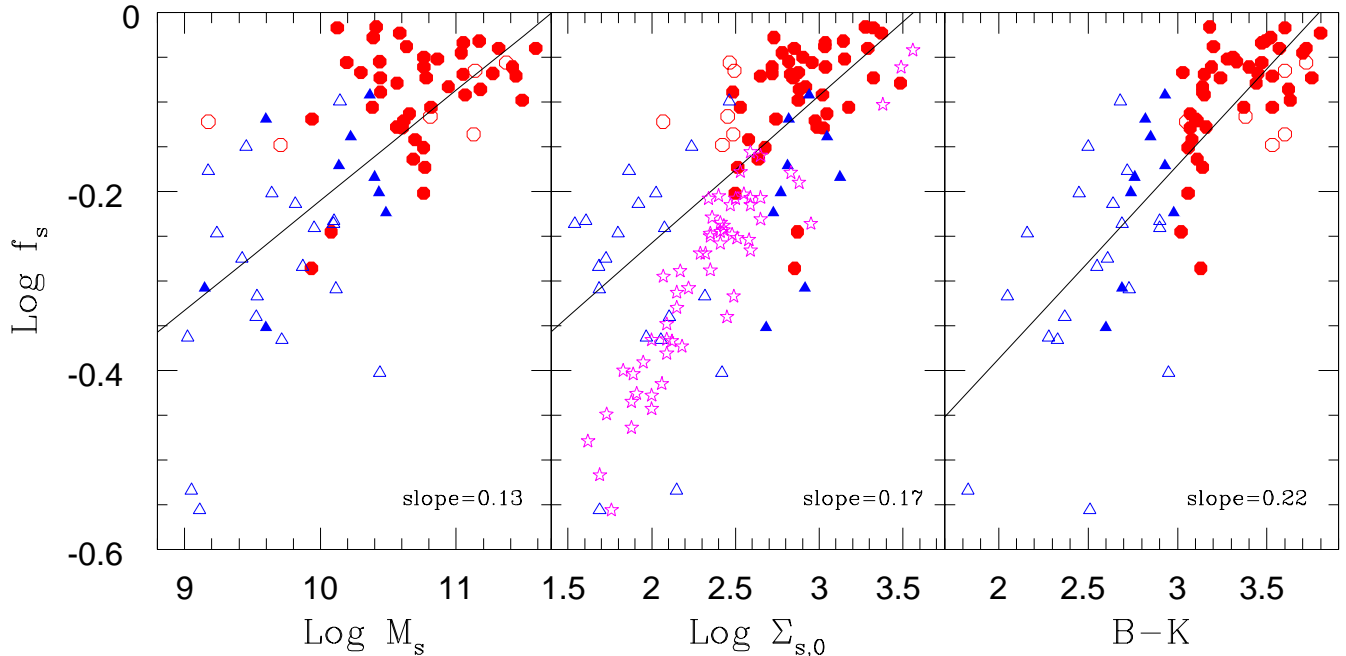


FIG. 7.— Stellar fraction f_s vs M_s , $\Sigma_{s,0}$, and $(B - K)$. Solid and empty symbols are for HSB and LSB galaxies, respectively. Red galaxies are represented with circles, while blue galaxies with triangles. The solid lines are the Log-Log orthogonal linear regressions. Stars are from models by FA-R.

in halos assembled earlier (more concentrated), are also shifted to the larger- M_s side because these galaxies had more time to consume their gas (they end up with higher f_s).

The predictions of the Λ CDM-based disk galaxy models provide an adequate context for interpreting the observational results plotted in the two upper rows of Fig. 6. The loss of dependence of the V_m - M correlation residuals upon the R - M correlation residuals when changing from baryonic to stellar quantities can be understood on the ground of the (self-regulated) SF efficiency dependence on disk surface density described above (see also Dutton et al. 2007). This also explains the reduction of the scatter around the TFR from the baryonic case to the stellar case (see Table 1), though the model results are more pronounced than observations both in the changes of the scatter values and in the slopes of the residual correlations.

In the same way, the distribution of galaxies in the diagrams of the residuals for the V_m - M , $(B - K)$ - M , and f_s - M correlations (Fig. 6) can be interpreted as follows. Upon the understanding that disk color and f_s are related mainly to the halo MAH (concentration), the correlations between the baryonic residuals $\Delta V_m(M_{\text{bar}})$ and $\Delta(B - K)(M_{\text{bar}})$, and between $\Delta V_m(M_{\text{bar}})$ and $\Delta f_s(M_{\text{bar}})$, are expected (see above). This is because for a given mass, halos assembled earlier have larger V_m , and the galaxies formed inside them transformed gas into stars earlier (therefore are redder) and more efficiently (therefore have higher values of f_s). In the corresponding panels of Fig. 6, one indeed sees these predicted tendencies, mainly for the HSB galaxies. For the LSB galaxies, the tendencies again (see §§3.4) almost disappear. It might be because the (low) SF rate in LSB galaxies no longer depend on the gas infall rate; this dependence is what allowed us to associate the observables,

color and f_s , to the halo MAH⁸. In the residual plots corresponding to stellar quantities, the tendencies become negligible because from M_{bar} to M_s , the shifts in V_m in the TFR, due to the halo MAH (concentration), tend to be compensated by shifts in M_s (see the previous paragraph). Therefore, in the V_m - M_s (stellar) diagram the mentioned SF effects tend to reduce the scatter and its dependence on surface density, color, and f_s compared to the V_m - M_{bar} (baryonic) diagram.

4.3. The luminous relations

The slopes and scatters of the K -band scaling correlations are similar, within the uncertainties, to those of the stellar scaling correlations. The only quantity that actually changes in the diagrams is L_K for M_s , through the K -band mass-to-luminosity ratio, Υ_K . This ratio increases slightly with the disk color for HSB galaxies and slightly decreases with it for blue LSB galaxies (§2.2). Hence, a significant trend of Υ_K with mass or V_m is not expected. For the scale length, we assumed that $R_s = R_K$.

Interesting differences are seen between the K - and B -band scaling correlations. In the V_m - L diagrams, the slope and intrinsic scatter increase significantly from the K to the B band. Calculating the ratio of the K - and B -band TFRs, we obtain: $(B - K) \propto V_m^\delta$, where δ is -2.5 times the difference of the B - and K -band slopes. This correlation is a consequence of the color- L correlation shown already in Fig. 5. That the less luminous galaxies systematically tend to be slightly bluer, implies already a steepening of the slope when changing from the K - to the B -band TFR.

⁸ Below a certain gas surface density, the SF rate could be so inefficient that its long scale-time becomes independent of the gas infall rate (given by the MAH). Alternatively, the SF rate in LSB galaxies could be disconnected from the gas infall rate and the gas surface density as a consequence of their low metal content, which makes the gas cooling very inefficient (Gerritsen & de Blok 1999).

Furthermore, the residuals of the B -band TFR are correlated with those of the $(B-K)$ - L_B correlation, and less with the residuals of the R_B - L_B and f_s - L_B correlations: redder galaxies, with higher SB and f_s tend to be shifted to the TFR large- V_m side; the opposite happens for bluer galaxies, with lower SB and f_s (lowest row panels in Fig. 6). In fact, the step-wise backward analysis mentioned in §§3.5 shows that the $(B-K)$ color is a statistically significant parameter in the V_m - L_B - $(B-K)$ multi-variable correlation, i.e. *color is the third parameter in the B -band TFR*, a result that other authors have also found in the optical bands (e.g., Verheijen & Sancisi 2001; Courteau et al. 2007; Kannappan et al. 2002, and more references therein). It is obvious that a galaxy in the V_m - L_K diagram shifts to the large (low) B -band luminosity side if it is bluer (redder) than the corresponding average.

Why do galaxies shifted to the high- (low-) V_m side in the B band TFR tend to be redder, with higher SBs and larger values of f_s (bluer, with lower SBs and smaller values of f_s)? According to the galaxy models discussed above, disks formed in halos with low λ and/or early mass assembling (high concentration), tend to consume gas into stars early in such a way that, for the same M_s or L_K , they result with older stellar populations (lower L_B and redder) and a higher f_s than those formed in halos with high λ and/or late mass assembling (low concentration). Thus, *while the dispersions introduced by λ , f_{gal} , and the MAH are reduced by compensating effects in the stellar and K -band TFRs (§§4.2), the opposite happens in the B -band TFR*. We see indeed that the TFR in blue bands is systematically more scattered than in the NIR bands (Table 1).

Regarding the R_B - L_B correlation, its slope is significantly steeper than that of the R_K - L_K correlation. Again this is because, as the galaxy is more luminous, it tends to be redder, i.e., the L_B -to- L_K ratio decreases with L . However, the situation is more complex than in the TFR case, because in the R - L diagrams (i) the scatter is large and galaxies are strongly segregated by SB and color, and (ii) the B - and K -band radii are not the same as is the case of V_m in the TFR diagrams; the R_B -to- R_K ratio tends to be larger for redder, more luminous galaxies. Thus, on one hand, the redder, higher SB galaxies shift to the low- L and high- R sides in the R - L diagram when changing from band K to band B ; the shift tends to be larger for the more luminous galaxies (see Fig. 2). On the other hand, the bluer, lower SB galaxies shift slightly, mainly to the low- L side, while the shift is larger for those of larger luminosities. As a consequence, the slope of the correlation increases in the B band and the scatter along the luminosity axis decreases.

In the V_m - R diagrams, the correlations do not significantly change when changing from the K to the B bands. This confirms that the most relevant shifts in the R - L diagrams are due to L rather than R . The models predict that the scatter around the V_m - R relation should thicken slightly in the band B with respect to the band K : galaxies of lower SBs and/or bluer (larger λ , late assembling halos, and lower f_{gal}), which are shifted to the low- V_m side in the K band, tend to shift also to larger B -band radii with respect to their R_K radii; for galaxies that are of higher SB and redder, the radii tend to be the same in both bands. According to Table 3, the direct

intrinsic scatter around the V_m - R_K and V_m - R_B correlations is almost the same, while the inverse scatter (along the R axis), is larger in the B band.

4.4. Quantitative comparisons

As shown, the predictions obtained with the Λ CDM-based models by FA-R offer an excellent qualitative description of several observational details of isolated disk galaxies. A systematic comparison of observations with results from models calculated with the most recent cosmological parameters will be presented elsewhere. With the aim to show that the models are able to provide even quantitative predictions, we plot those results from FA-R that can be compared with the observational inferences presented here. In FA-R, the authors plotted averages and scatters for three mass bins in the stellar TFR diagram (their Fig. 7), that we reproduce here in the corresponding panel of Fig. 1 (magenta stars with vertical error bars). We diminished their M_s points by the factor $(0.70/0.65)^{-2}$ in order to take into account the slightly different value of H_0 used in their models. The agreement is good, even more if we consider that models calculated with a $\sigma_8 < 1$, would have smaller values of V_m . The agreement is also quite good in the baryonic TFR diagram (magenta stars in the lower right panel of Fig. 1; the f_g values given in FA-R were used to calculate M_{bar} from M_s). It should be stressed that models and observations are now being fairly compared; in both cases we have nearly isolated normal disk galaxies in a wide range of SBs and morphological types.

In FA-R, model results for the R_s - V_m relation were also presented, separated in HSB and LSB galaxies, but models with very high SB were not taken into account. We estimate the “weight” of these models in the fit for the HSB galaxies, and reproduce both the LSB and HSB+very HSB fits in the corresponding panel of Fig. 3 (thick magenta dashed lines), correcting the radii by a factor of $(0.70/0.65)^{-1}$. The agreement is rather good within the large scatter. Finally, model results by FA-R in the f_s - $\Sigma_{s,0}$ diagram (Fig. 7, magenta stars), and (ii) in the diagram of residuals of the baryonic V_m - M_{bar} and R_{bar} - M_{bar} correlations (upper left panel of Fig. 6, magenta dashed line) were already presented above, evidencing a reasonable agreement with observations; for the stellar case, the residuals do not correlate, as seen also for the observations.

5. POSSIBLE DIFFICULTIES FOR THE DISK Λ CDM-BASED MODELS

The hierarchical Λ CDM-based models of disk galaxy evolution discussed above have been useful for interpreting the results reported in §3 about the slopes and scatters of the observed scaling relations in the different cases, as well as the behaviors of the residuals from these and other correlations. Even the zero-points of the relations predicted by FA-R seem to agree quantitatively with observations. Note that the models by FA-R, differentiate from others in the literature in that they *include a detailed description of disk SF and feedback and follow self-consistently the whole process of halo-disk evolution*. Although a detailed comparison with observations, using models calculated with more recent cosmological parameters, was left for a forthcoming paper, we may anticipate

here some potential shortcomings of the model predictions as well as solutions.

(1) *The models are not able to explain the observed correlation of galaxy color with mass or luminosity.* In the hierarchical scenario, isolated more massive halos tend to assemble a given fraction of their present-day mass later than the less massive ones. Then disks formed inside the more massive halos would tend to be younger (bluer) than those formed in the less massive halos. However, the models also show that the more massive the halo is, the higher the surface density of the disk formed inside it (Dalcanton et al. 1997; FA-R); the higher the disk surface density, the more efficient the SF process and therefore, the redder the galaxy. As a result of these two evolutionary compensating effects, the models predict almost no dependence of color on M or L (e.g., Avila-Reese & Firmani 2000; Avila-Reese et al. 2005, see Table 5 therein). A possible way to produce a steeper color- M correlation in the models is by obtaining a steeper disk surface density- M dependence; in fact, the model prediction for this dependence is also too shallow as compared with observations (see below). It should be said that the models do not include satellite galaxies and interacting-induced SF. For massive systems it is probable that the late gas infall is reduced by the large cooling time and because a fraction of the gas could have been trapped before into substructures that tend to be incorporated into the central galaxy through (minor) mergers; all these processes make the most luminous galaxies redder and with larger f_s values than obtained in the FA-R models.

An indirect dependence of galaxy color on L may also appear through environment. However, the disk galaxy sample studied in this paper includes field galaxies and galaxies from the UMa low-density, low mass cluster of galaxies. Therefore, it is less probable that environmental effects should produce the color- L correlation. This correlation, which in some sense resembles the so-called *anti-hierarchical or downsizing galaxy formation* reported for early-type luminous galaxies (e.g., Cimatti, Daddi & Renzini 2006), could be produced by a mass (luminosity)-dependent dust extinction larger than that used here to correct the observations. Another alternative is related to the AGN feedback mechanism invoked recently to solve the sharp cut-off at the high-end of the (elliptical) galaxy luminosity function, as well as the observed downsizing of red early-type galaxies (e.g., Bower et al. 2006). Such a mechanism should be, however, strongly dependent on the galaxy mass in order to produce the observed continuous and monotonic change of color with mass (luminosity) of disk galaxies.

(2) *The predicted dependence of surface density on mass (or SB on luminosity) is too shallow as compared to that inferred from observations,* although the latter is very noisy. Such a dependence can be estimated by combining the two simple model relations:

$$R_{\text{bar}} \propto \lambda g(c) R_{\text{h}} \propto \lambda g(c) (M_{\text{bar}}/f_{\text{gal}})^{1/3}, \quad (5)$$

$$R_{\text{bar}} \propto (M_{\text{bar}}/\Sigma_{\text{bar},0})^{1/2}.$$

By rejecting the small dependence of $g(c)$ on mass (see Appendix C2), we then obtain that

$$\Sigma_{\text{bar},0} \propto M_{\text{bar}}^{1/3} f_{\text{gal}}^{2/3} / \lambda^2. \quad (6)$$

The semi-numerical evolutionary models show that the dependence of $\Sigma_{\text{bar},0}$ on M_{bar} is even shallower than

1/3. On the other hand, the slope (orthogonal regression) that we have found for the (noisy) correlation between $\Sigma_{\text{bar},0}$ and M_{bar} in our galaxy sample is ~ 0.7 , and it does not change significantly for the stellar and luminosity cases. Assuming that there is no a dependence of f_{gal} and λ on mass, model predictions and observations would not agree: the surface density (brightness) of observed galaxies increases on average more rapidly with M (L) than the models predict. Again, the inclusion of mergers and interaction-induced SF would work in the direction of increasing $\Sigma_{\text{s},0}$ in the more massive galaxies.

On the other hand, recent inferences of the halo λ distribution for a large SDSS sub-sample of galaxies show this parameter to be systematically smaller and less scattered for more luminous galaxies (Cervantes-Sodi et al. 2007; Berta et al. 2008; see also Hernandez et al. 2007). By taking into account an anti-correlation of λ with mass in the models, both the color (1) and surface density (2) problems could be ameliorated without affecting significantly the scaling correlations. The question is why more massive galaxies would end with smaller values of λ –and consequently, higher surface densities– than the less massive ones. Cervantes-Sodi et al. (2007) suggested that the trend of λ with mass can be related to the halo angular momentum acquisition. A complementary explanation may lie in the baryon processes. For example, the outer gas in the most massive galaxy halos may not have enough time to cool and fall to the disk (for numerical results see e.g., van den Bosch et al. 2002; Keres et al. 2005); the material located in the outer regions is the richest in the specific angular momentum (Bullock et al. 2001b). On the other hand, in less massive halos the outer gas may flow through filaments to the disk, even before being shock-heated by the halo collapse (Keres et al. 2005). As a result, the specific angular momentum content will be higher in low mass galaxies and lower in the massive ones, which implies lower and higher disk surface densities, respectively. Note that this scenario also implies that more massive galaxies would tend to have lower values of f_{gal} . A mild anti-correlation of f_{gal} with mass in the models is allowed according to the observational results presented here (§§4.1): the $V_{\text{m}}-R_{\text{bar}}$ relation would agree with the anti-correlation, while the $R_{\text{bar}}-M_{\text{bar}}$ relation would do so in case λ also anti-correlates with mass, and regarding the $V_{\text{m}}-M_{\text{bar}}$ relation, there is room for a mild variation of f_{gal} with mass. Detailed model calculations are necessary for obtaining more quantitative conclusions.

(3) *Are the scatters around the model and observed TFRs in agreement?* For the baryonic case, the agreement is marginal, given the scatter in the models is slightly larger than that in the observations (§§4.1). The difference could be even larger if (i) some of the simplifying assumptions introduced in the models are relaxed, which would increase the predicted scatter, and/or (ii) systematic errors such as disk ellipticity are present, which would give rise to a reduction in our estimate of the observational intrinsic (physical) scatter⁹. Therefore, the current models of disk galaxy formation based on

⁹ Some researchers have found evidence that disk ellipticity could account for roughly 50% of the observed scatter in the luminous TFR (Andersen et al. 2001; see also Franx & de Zeeuw 1992; Rix & Zaritsky 1995) or it could even explain all the observed scatter (Ryden 2004).

the Λ CDM cosmology have a potential problem in predicting the intrinsic scatter around the baryonic TFR. This scatter is smaller in the models for lower values of f_{gal} or for a distribution of λ narrower than that of the Λ CDM halos. It could also be possible that the potential systematic errors, such as disk ellipticity, confabulate with the disk surface density or baryonic-to-total mass ratio (with λ and f_{gal} from the model's point of view) in such a way that the observed TFR scatter is systematically diminished.

For the stellar case, the scatter in the models becomes slightly smaller than that in the observations (§4.2). Although in both cases (models and observations), the scatter decreases from the baryonic TFR to the stellar TFR, for models, the decrease is more pronounced than it is for observations. However, there are known effects not considered in the FA-R models, like the interaction-induced SF, that will work certainly in the direction of increasing the scatter around the stellar TFR (e.g., Barton et al. 2007), but not around the baryonic one.

(4) *Are current models able to match both the TFR zero-point and the galaxy luminosity function?* First, we note that the disk galaxy evolutionary approach, like the one of FA-R, is different by construction to the semi-analytic models (SAM) or the halo occupation models (HOM): the former is focused on the modeling of the galaxy internal physics and evolution, while the latter are constructed for reproducing galaxy population global properties as the luminosity function. The parameters that the SAM and HOM need for reproducing in detail the observed luminosity function apparently produce a luminous TFR whose zero-point is shifted to the higher-velocity side with respect to observations (Baugh 2006, and references therein). Some astrophysical solutions were proposed to alleviate this apparent problem (e.g., Dutton et al. 2007; Gnedin et al. 2007).

However, before introducing modifications to the common disk galaxy formation scenario, we may mention at least four aspects that should be taken into account in order to compare fairly the predictions of SAM/HOM with observations in regards to the TFRs. (1) Since the TFRs are related to internal disk properties, a more detailed modeling of these properties than that carried out in the SAM is necessary; for example, in the SAM, disks are assumed to have a purely exponential mass distribution, the SF-feedback processes are artificially linked to the halo circular velocity, etc. (2) V_m is typically used to define the TFRs, while in the SAM/HOM only approximations to this velocity are calculated. (3) The TFRs refer only to the population of normal disk galaxies, while the luminosity function that the SAM/HOM fit to observations refers to the overall galaxy population. (4) The halos where disk galaxies form could be a subgroup of the overall halo population, for example those that did not suffer a major merger since $z \sim 1$; therefore, the corresponding “disk galaxy” halo mass function, and not the overall one, should be used in the HOM as the starting point in the procedure of shaping the luminosity function.

From the point of view of the SAM and HOM, the passage from the halo mass function to the galaxy luminosity function implies a specific M_h -to- L ratio as a function of mass. Recent studies using galaxy-galaxy weak lensing, allowed one to directly determine the ‘cen-

tral’ galaxy M_h -to- L ratios (e.g., Hoekstra et al. 2005; Mandelbaum et al. 2006). For the FA-R models, which would agree very well with the baryonic and stellar TFRs if corrected for $\sigma_8 < 1$, we have the B -band luminosities available. The results from Mandelbaum et al. (2006) for *late-type* galaxies (note that they differ from those of the early-type galaxies) are given in the r band. By using $\langle (B - R) \rangle = 1.2$ for late-type galaxies (de Jong 1996b) and $(r - R) = 0.2$, we estimate from the FA-R models $\langle M_h/L_r \rangle / (M_\odot/L_{r,\odot}) = 62.2 \pm 9.1, 60.7 \pm 14.3, \text{ and } 77.6 \pm 26.5$, for the luminosities $\langle L_r \rangle / L_{r,\odot} = (5.6 \pm 1.1) \times 10^{10}, (5.7 \pm 1.2) \times 10^9$, and $(4.85 \pm 1.2) \times 10^8$, respectively. To compare the FA-R M_h/L_r ratios with those of Mandelbaum et al., the values just reported should be increased by $\approx 15\%$ due to the different definitions of M_h . The good agreement between the models and observations within their scatters is encouraging. The model predictions also agree roughly with the $\langle M_h/L_r \rangle$ and $\langle M_h/M_{\text{bar}} \rangle$ ratios calculated from the observed luminosity function and the stellar mass-to- L ratios inferred from kinematical mass modelling (Shankar et al. 2006). We can also compare tracers of the inner luminous (or baryonic)-to-dark matter ratios of models and observed galaxies. For example, in ZAHF the disk-to-total velocity ratio at the maximum of the rotation curve was estimated for the same galaxies studied here. The models and observations were found to agree roughly, both in the zero point as well as in the dependence of this ratio on the disk surface density or SB (see Fig. 3 in ZAHF).

Summarizing, the FA-R models based on the Λ CDM scenario seem to be able to predict both the TFR, including its zero point, and the inferred, directly from observations, M_h -to-luminosity ratios of central late-type galaxies, as well as the inner luminous and baryonic-to-dark matter contents. These ratios, specially the former, are closely related to the “transfer” function needed for passing from the halo mass function to the galaxy luminosity function. We speculate that if the SAM and HOM take into account the shortcomings mentioned above, then the potential problem of fitting both the TFR zero point and the luminosity function will be overcome. On the other hand, some of the initial condition parameters used in models such as those of FA-R, if any, could be modified accordingly to reproduce the disk-galaxy luminosity function, while the TFRs (and the other scaling relations) would be yet in agreement with the observations. For example, the anti-correlation of f_{gal} with mass for luminous galaxies (motivated by the large cooling time in massive halos) that the SAM/HOM evoke, could be allowed by the models as discussed in items 1 and 2 above.

6. SUMMARY AND CONCLUSIONS

A compiled sample of 76 normal (non-interacting) local disk galaxies of all morphological types and SBs has been used to construct and compare, among them, the luminous (bands B and K), stellar and baryonic scaling relations. The required observational information for building up this sample implied detailed surface photometry in bands B and K , a dynamical determination of the rotation curve amplitude, and HI gas integrated flux data. We have corrected and processed the observational data homogeneously, and obtained several compos-

ite disk quantities and their uncertainties: global ($B-K$) colors, stellar masses and surface densities, gas (or stellar) fractions, and baryonic masses, surface densities and scale lengths. The objectives of this work were (i) to explore the changes of the disk–galaxy scaling relations and their residuals as moving from optical to NIR bands, and to stellar and baryonic quantities, (ii) to look for interpretations of the results in the context of Λ CDM–based evolutionary disk–galaxy models, and (iii) to show the necessity of larger samples, similar to the one compiled here, for constraining models of galaxy formation and evolution. A summary of the results is as follows.

- The slope of the baryonic TFR is shallower than the slopes of the stellar and K –band TFRs (≈ 0.31 vs ≈ 0.27 and 0.26 ; orthogonal regression) and, in agreement with previous works, the slope of the B –band TFR is steeper than that of the K –band TFR (≈ 0.32 vs ≈ 0.27). The estimated average intrinsic scatters in $\log V_m$ around the baryonic, stellar, K – and B –band TFRs are 0.051 , 0.045 , 0.049 , and 0.063 dex, respectively. Thus, the baryonic TFR is more scattered than the stellar TFR. A statistical analysis shows that the radius (or surface density) is a significant third parameter in the former relation, while the latter, as well as the K –band TFR, do not admit a third parameter. In the case of the B –band TFR, which is the most scattered, the ($B-K$) color is a significant third parameter.

- The R – M (– L) correlations are scattered and segregated strongly by disk SB and weakly by color. The slopes of the baryon, stellar, and K –band correlations are around 0.30 (orthogonal regression), while for the B –band relation, this increases to 0.44 . The scatter around the latter, projected in the luminosity axis, is smaller than that in the other correlations. The $V_m - R$ correlations are the most scattered and are also segregated strongly by disk SB and less by color. The slopes have values of around 0.5 .

- The residuals of the baryonic V_m – M_{bar} and R_{bar} – M_{bar} correlations are anti-correlated, mainly for the HSB galaxies. The slope is -0.15 ± 0.04 (orthogonal regression), showing that the smaller the disk radius, for a given mass (higher surface density), the larger the disk contribution to V_m . For the stellar and K –band cases, the anti-correlation almost disappears. Thus, our results show that the correlations among the mentioned residuals are different for the baryonic, stellar, K – and B –band cases. While the correlation (or the lack of it) among the residuals in the baryonic case can be used to explore the dynamical importance of the halo/disk in galaxies, in the stellar and luminous cases the effects related to SF processes distort any pure dynamical interpretation of the results.

- In spite of the velocity–dependent internal extinction correction that we have applied, the ($B-K$) color correlates significantly with the logarithms of L_B , L_K , M_s , and M_{bar} (orthogonal regression slopes of 0.61 , 0.53 , 0.56 , and 0.60 , respectively). Noisy but steep correlations are observed between the surface densities and brightnesses and the corresponding masses and luminosities. The stellar fraction, f_s , correlates strongly with ($B-K$) and less with surface densities (brightnesses) and luminosities (masses). In all cases, the lowest SB galaxies break the latter correlations, suggesting a kind of threshold in the surface density, below which the SF rate is almost

independent of it (and of M or L) and of the gas infall rate.

We have discussed previous models of disk–galaxy formation and evolution (including halo contraction, SF, and disk feedback; e.g., FA-R) within hierarchically growing Λ CDM halos, under the assumption of gas–detailed angular momentum conservation. We showed the potentiality of these models to describe the observational inferences, as well as how such inferences can help us to constrain several of the model parameters. A crucial aspect of this endeavor is the correct comparison of models with observations. The basic models refer to isolated normal disk galaxies. Therefore, the observational sample should also be for nearly isolated normal disk galaxies. We highlight the following conclusions:

- The slopes of the baryonic V_m – M_{bar} , R_{bar} – M_{bar} , and V_m – R_{bar} correlations can be interpreted as a direct imprint of the cosmological Λ CDM halo $V_{m,h}$ – M_h , R_h – M_h , and $V_{m,h}$ – R_h relations, especially the former (baryonic TFR), which is the tightest one. The models show that this relation is robust to systematical or statistical variations in the disk baryonic mass fraction, f_{gal} , for $f_{\text{gal}} < 0.08$. Then, the main sources of scatter are the dispersions in the halo spin parameter λ and halo MAH (or concentration). The FA-R models provide a lower limit to the scatter around the relation due to these two dispersions, namely $\sigma_{\text{intr}}(\text{Log} V_m) \approx 0.053$ ($f_{\text{gal}} = 0.05 = \text{const.}$), which is already slightly larger than our observational inference.

- In combination, the slopes and scatters of the baryonic V_m – M_{bar} , R_{bar} – M_{bar} , and V_m – R_{bar} correlations inferred here from observations, as well as the correlations among their residuals, imply that the average value of f_{gal} in normal disk galaxies could not be larger than ~ 0.05 and that f_{gal} can not depend strongly on M (or L); if any, a moderate anti-correlation with M is permitted. A trend of f_{gal} nearly independent on mass, with average values of $f_{\text{gal}} < 0.05$, has been reported recently by other authors, who extended the analysis to disk dwarf galaxies and inferred halo masses directly from the observational data (Blanton et al. 2007; see also Baldry et al. 2008; Begum et al. 2008).

- The models are able to explain qualitatively the observed (weak) anti-correlation among the residuals of the baryonic V_m – M_{bar} and R_{bar} – M_{bar} correlations and the related finding that the radius (or surface density) is a third parameter in the former correlation. The physical parameter beyond these behaviors is λ . Model disks with low λ have high surface density and contribute significantly to V_m , in such a way, that for a given mass, V_m correlates with R_{bar} or $\Sigma_{\text{bar},0}$. Instead, disks with high λ values are of low surface density and have a negligible gravitational contribution to V_m ; then, the dependence of V_m on $\Sigma_{\text{bar},0}$ (or on R_{bar} for a fixed mass) tends to disappear. The models can also explain why the anti-correlation among the residuals becomes negligible in the stellar or K –band cases: for a given mass, galaxies not only shift to the high- V_m side in the TFR diagram as the radius is smaller ($\Sigma_{\text{bar},0}$ is higher), but also shift to the high- M_s (or L_K) side due to a higher efficiency in transforming gas into stars. As a result, the scatter around the stellar TFR becomes independent of R_s or $\Sigma_{s,0}$, and smaller than in the baryonic case.

- The (self-regulated) SF efficiency effect just men-

tioned produces a dependence of the stellar mass fraction f_s on surface density (or brightness). Such a non-trivial prediction roughly agrees with the one found for our processed galaxy catalog (Fig. 7), and it is associated mainly with the λ parameter: the smaller the λ , the higher the disk surface density and the more efficient the transformation of gas into stars. Although less relevant, f_s and $\Sigma_{s,0}$ are also affected by the gas infall history, which is connected to the cosmological halo MAH. Since the MAH plays a role in the scatter of the baryonic TFR, trends among the residuals of this relation and those of the color- M_{bar} and f_s - M_{bar} relations are predicted. These trends were found for our observational catalog, mainly for the HSB galaxies (Fig. 6). For LSB galaxies, it could be that the SF-rate timescale becomes larger than the that of the gas infall rate, the connection between MAH and color/ f_s then disappears.

• *Potential difficulties.*— Our observational results show that both (i) the color- M and (ii) surface density- M correlations are steeper than the models would predict. We speculate that these shortcomings suggest that late minor mergers and interaction-induced SF, which are more common in massive galaxies, should play some role and/or that both, the galaxy spin parameter and f_{gal} anti-correlate with mass; at least qualitatively, both anti-correlations, in combination are not expected to affect the scaling correlations presented here. (iii) The fact that the intrinsic scatter around the predicted baryonic TFR appears to be larger than that inferred here, implies that there is no room for other physical or systematical sources of scatter around the TFR such as disk ellipticity. On the other hand, the intrinsic scatter around the stellar TFR becomes smaller in the models than in the observations. However, external effects, such as the interaction-driven SF, work in the direction of adding some scatter to the stellar TFR. (iv) The FA-R models (rescaled to $\sigma_8 < 1$) agree with the observed baryonic and stellar TFR zero points as well as with the M_h -to- L ratios inferred directly from observations. The potential difficulty that the SAM/HOM find in matching both the TFR zero point and the luminosity function could be solved by taking into account the shortcomings we have discussed in §5.

The results obtained in this work pose relevant questions for future studies. We showed that the determination of the scaling relations for disk galaxies in different bands and for stellar and baryonic quantities, as well as for the correlations among their residuals, bring valuable information on the nature and evolution of galaxies. The completion of large galaxy samples, unbiased and broad in properties, with detailed photometric, dynamic, and gas-content information is crucial for this kind of study. The preferred approaches for such an undertaking are: follow-up observations in H_α and/or HI emission lines for galaxies from the largest optical/NIR band surveys as SDSS (Pizagno et al. 2005), and synergy of existing wide-area homogeneous surveys conducted at optical/NIR bands and HI emission line, for example SDSS with HI surveys such as ALFALFA (Giovanelli et al. 2005). According to the philosophy followed in this paper, substantial advance comes from the adequate comparison of observations with theoretical models. Thus, in order to confirm, rule out, or perhaps expand, some of the conclusions attained here, a deep model exploration

of the formation and evolution of the disk galaxy population should be carried out.

This work was supported by PAPIIT-UNAM grant IN107706 to V.A. and CONACyT grant 42810 to H.M.H. J. Z. acknowledges support from DGEP-UNAM and CONACyT scholarships, and support by the CAS Research Fellowship for International Young Researchers. J. Z. is supported by the Joint Program in Astrophysical Cosmology of the Max Planck Institute for Astrophysics and the Shanghai Astronomical Observatory. We are grateful to S. Courteau for comments to an early version of the manuscript and to the anonymous referee for his/her criticism and suggestions.

APPENDIX A: ERROR BUDGET

In the following we describe how we estimate the uncertainties for the quantities we used to construct the scaling relations presented along the paper. We assume them to be Gaussian distributed, so our estimates refer to the standard deviation.

B and K magnitudes: we neglect the contributions to the errors due to uncertainties on the redshift, the extinction in our Galaxy, the disk thickness, and the k correction. Hence, the square of the error in the absolute magnitudes is estimated as the quadratic sum of the measurement error, ϵ_m (given in the original papers used to compile the sample), and the one due to the correction for internal extinction, ϵ_{A_i} :

$$\epsilon_{M_{abs}}^2 = \epsilon_m^2 + \epsilon_{A_i}^2, \quad (7)$$

To estimate ϵ_{A_i} we take into account only errors related to the inclination of the galaxies, $\epsilon_{b/a}$, and neglect errors related to the empirical parameter γ (recall that $A_i = \gamma(W_{20})\log(b/a)$, Tully et al. 1998). Giovanelli et al. (1997) suggest to add also the error $\epsilon_\gamma = 0.15\gamma$, but this term is in most of the cases sub-dominant compared to the error in the inclination (see, for instance, fig. 2 of their paper); only for high inclination and high values of γ both terms may become comparable. Thus, we have

$$\epsilon_{A_i} = \left(\frac{0.434}{b/a}\gamma\right)\epsilon_{b/a}, \quad (8)$$

where we assume $\epsilon_{b/a} = 0.09 - 0.12(1 - b/a) + 0.037(1 - b/a)^2$, following the estimation for the median error of $\epsilon_{b/a}$ given by Giovanelli et al. (1997). Finally, the error in $\log L$ is given by $\epsilon_{\log L} = \epsilon_{M_{abs}}/2.5$, where $\epsilon_{M_{abs}}$ was given in equation (7).

Stellar mass: The error in $\log M_s$ is estimated as the quadratic sum of the logarithmic errors in L_K and in the mass-to-luminosity ratio Υ_K :

$$\epsilon_{\log M_s}^2 = \epsilon_{\log L_K}^2 + \epsilon_{\log \Upsilon_K}^2, \quad (9)$$

where an uncertainty of 25% in the value Υ_K was considered (Bell et al. 2003a).

Baryonic mass: The error is calculated as the quadratic sum of the errors in M_s and M_g , $\epsilon_{M_{\text{bar}}}^2 = \epsilon_{M_s}^2 + \epsilon_{M_g}^2$; the corresponding logarithmic error in M_{bar} is then

$$\epsilon_{\log M_{\text{bar}}} = \frac{0.434}{M_{\text{bar}}}\epsilon_{M_{\text{bar}}}. \quad (10)$$

The error in M_g is calculated as:

$$\epsilon_{M_g} = M_g \frac{\epsilon_{S_\nu}}{S_\nu}, \quad (11)$$

where the measurement error ϵ_{S_ν} is taken as reported in the HyperLEDA information system.

Scale lengths: In order to estimate the fitting error in the scale lengths of the galaxies used here, we have experimented with the fit of the observed SB profiles by using both a marking–the–disk method and the bulge–to–disk decomposition method. We have seen that typical uncertainties in the determination of R by both methods are of the order of 5 – 10% (see also MacArthur et al. 2003; Graham 2002). There is a very weak systematical trend for larger lengths determined by the latter method relative to those determined by the former one from late to early morphological types. The uncertainty in R also depends on the SB profile type and other specific details. Finally we decided to assign a logarithmic error of $\epsilon_{\log R} = 0.05$ ($\approx 11\%$) to the scale lengths in both the B and K bands, and $\epsilon_{\log R} = 0.06$ to the baryonic case, where the gas disk also contributes to the final surface density profile.

Rotational velocities: The errors (standard deviations) in $\log W_{20}$, $\epsilon_{\log W_{20}}$, were taken from the sources, namely Verheijen (1997), Verheijen & Sancisi (2001), and the HyperLeda information system.

APPENDIX B: THE SCALING RELATIONS OF CDM HALOS AND DISK GALAXY FORMATION

Distinct CDM halos –those not contained within larger halos– can be characterized by the so-called virial mass and radius, M_{vir} and R_{vir} , and by a maximum circular velocity, $V_{\text{m,h}}$. Halos which are contained inside larger ones (sub-halos) commonly have radii and masses smaller than R_{vir} and M_{vir} , because their growth is truncated or even reversed due to tidal stripping; $V_{\text{m,h}}$ is less affected by these effects. It is well known that the masses and maximum circular velocities of CDM halos, and even of sub-halos, correlate tightly as $V_{\text{m,h}} \propto M_h^a$ with $a \approx 0.32 - 0.30$, where M_h is the virial or truncated mass of the halo (e.g., Navarro et al. 1997; Avila-Reese et al. 1998, 1999, 2005; Bullock et al. 2001a). The correlation is basically an imprint of the linear power spectrum of fluctuations, whose variance at the galaxy scales decreases very slowly (logarithmically) with the fluctuation mass. This rough scale invariance naturally produces the $V_{\text{m,h}}-M_h$ relation for the collapsed CDM halos. The complex non-linear non-spherical hierarchical halo assembly process introduces only minor deviations upon this relation as well as a scatter. The cosmological TFR has an intrinsic scatter, $\sigma_{\text{MAH}}(\text{Log}V_{\text{m,h}})$, mainly due to the stochastic nature of the mass assembly histories, which also produces a scatter in the halo concentration parameter c (Avila-Reese et al. 1998, 1999; FA-R).

For distinct halos, by definition $R_{\text{vir}} \propto M_{\text{vir}}^{1/3}$; sub-halos tend to follow a similar relation between R_h and M_h , but with some scatter and with a smaller proportionality coefficient. Consequently, $V_{\text{m,h}}$ and R_h are also correlated, as $V_{\text{m,h}} \propto R_h^\gamma$ with $\gamma \approx 1 - 1.25$, although extra scatter is introduced in this relation due to the variation in $V_{\text{m,h}}$ for a given mass, as in the case of the $V_{\text{m,h}}-M_h$ relation.

Disk galaxies are assumed to form inside the growing CDM halos from the trapped baryons. Therefore, the scaling relations of the halos are expected to be imprinted in the baryonic and stellar scaling relations of disk galaxies. We describe below the main physical ingredients of the FA-R models (see for details Avila-Reese et al. 1998; FA-R; Avila-Reese & Firmani 2000). An extended Press–Schechter approach is used to generate the MAHs of the halos from the primordial density fluctuation field, and a generalized secondary infall model is applied to calculate the time–by–time virialization of the accreting mass shells. The evolution and structure of the Λ CDM halos calculated in this way agree well with results from cosmological N–body simulations (Avila-Reese et al. 1999). The halo mass shells are assumed to have aligned rotation axis with specific angular momentum given by $j_{sh}(t_v) = dJ(t_v)/dM_v(t_v)$, where $J = \lambda GM_v^{5/2}/|E|^{1/2}$, J , M_v and E are the total angular momentum, mass, and energy of the halo at the shell virialization time t_v . The halo spin parameter, λ_h , is assumed to be constant in time. As a result of the assembling of these mass shells, a present day halo ends with an angular momentum distribution close to the (universal) distribution measured by Bullock et al. (2001b) in N–body simulations.

A fraction f_{gal} of the mass of each shell is assumed to cool down and form a disk layer in a dynamical time. The radial mass distribution of the layer is calculated by equating its specific angular momentum to that of its final circular orbit in centrifugal equilibrium (detailed angular momentum conservation is assumed). The superposition of these layers form the disk, which tends to be steeper in the center and flatter at the periphery than the exponential law. The disk surface density distribution is mainly determined by the halo angular momentum distribution. For example, for a given halo of radius R_h and mass M_h , the characteristic size of the baryonic disk (and its typical surface density), described in a first approximation by the scale length, R_{bar} , is determined mainly by the halo spin parameter, λ_h . The distribution of λ_h found in analytical and numerical studies is well described by a log-normal function, whose median and dispersion almost do not depend on the halo mass. While we assume here that the pre- and post-disk formation spin parameters are equal, $\lambda_h = \lambda_d$, in most of our discussions, the quantity λ refers to the post-disk formation spin parameter and it could deviate from λ_h if the baryon angular momentum is redistributed (in the halo or inside the disk) or if not all the halo gas falls into the disk.

The gravitational interaction of disk and inner halo (important for estimating V_m) is calculated using an extended adiabatic invariance formalism, which differs from the usual one in that we take into account the ellipticity of the orbits, i.e., the circular orbit assumption is relaxed. The disk SF at a given radius (azimuthal symmetry is assumed) is triggered by the Toomre gas gravitational instability criterion and self-regulated by a vertical disk balance between the energy input due to SNe and the turbulent energy dissipation in the ISM. This physical prescription naturally yields a Schmidt law with an index $n \lesssim 2$, varying slightly along the disk. The SF efficiency depends on the gas surface density determined mainly by λ , and on the gas accretion rate determined by the

cosmological MAH. Finally, we estimate the mass of the (pseudo)bulge as the inner disk mass where the Toomre stellar parameter indicates disk instability.

APPENDIX C: PREDICTIONS FOR THE BARYONIC SCALING RELATIONS

C.1. The V_m - M_{bar} relation

In order to pass from the cosmological TFR to the baryonic one, we should pass (i) from the halo $V_{m,h}$ to V_m , and (ii) from the halo mass M_h to M_{bar} . The latter is given simply by $M_{\text{bar}} = f_{\text{gal}} M_h$, where f_{gal} is the (central) galaxy mass fraction. The distribution of f_{gal} and its possible dependence on M_h and other halo properties is not well known. However, indirect and direct pieces of evidence show that f_{gal} should be much smaller than the universal baryon fraction, $f_{\text{gal}} \ll \Omega_b / \Omega_{\text{dm}}$ (e.g., Mo et al. 1998; FA-R; Smith et al. 2001; Bell et al. 2003b; Jiménez, Verde & Oh 2003; Pizagno et al. 2005; Hoekstra et al. 2005; Mandelbaum et al. 2006; Blanton, Geha & West 2007). Regarding item (i), the formation of the disk inside the dark halo and the gravitational drag produced on it, redistributes the inner mass profile. The $V_m / V_{m,h}$ ratio increases with the disk surface density and the disk baryon fraction f_{gal} . For a given M_h , the disk has a larger surface density for a smaller value of λ . Therefore, the relation between $V_{m,h}$ and V_m depends on both λ and f_{gal} : $V_m / V_{m,h} = G(\lambda, f_{\text{gal}})$. The function $G(\lambda, f_{\text{gal}})$ has been approximated in Zavala (2003) from models of disk formation inside CDM halos based on Mo et al. (1998) and FA-R (note that FA-R used an adiabatic contraction formalism generalized for elliptical orbits; as a result, the contraction is weaker than in the simpler case of circular orbits; see also Gnedin et al. 2004). If λ and f_{gal} do not depend on mass, then the function G is almost independent of mass, and then the baryonic TFR is expected to have a slope similar to the cosmological TFR. On the other hand, due to the gravitational disk-halo coupling, as f_{gal} decreases, G also decreases in such a way that the objects in the baryonic TFR diagram shift nearly parallel to the cosmological TFR. The function G becomes more sensitive to λ as f_{gal} becomes larger; for higher values of f_{gal} , a large variation in G is expected. This has deep implications for the scatter in the baryonic TFR.

The intrinsic scatter in the baryonic TFR has at least three sources: (i) the original scatter from the halo cosmological TFR, (ii) the scatter in V_m due to the dispersion in λ , and (iii) the scatter in both V_m and M_{bar} due to the average value and dispersion of f_{gal} . As mentioned above, the latter produces a shift of the models nearly along the same relation, in such a way that its effect on the baryonic TFR scatter is expected to be small for reasonably average values of f_{gal} ($\lesssim 0.08$). The major contribution to the scatter comes from the dispersion in the spin parameter λ . For a given f_{gal} and $V_{m,h}$, different values of λ produce disks of different surface densities, and therefore different values of V_m ; such an effect is accounted for by the function G . For a given distribution of λ , the scatter due to λ , σ_λ , increases as f_{gal} increases. The scatter also increases slightly if we allow for a dispersion in f_{gal} around the mentioned values (Gnedin et al. 2007). The scatter in the halo $V_{m,h}$ - M_h relation, $\sigma_{\text{MAH}}(\text{Log} V_{m,h})$, arises because halos of a given mass that

were formed through a rapid mass assembling process are more concentrated and have a larger $V_{m,h}$ than those that assembled slowly (Avila-Reese et al. 1998,1999). The magnitude of this scatter slightly decreases with mass and has a value of $\sigma_{\text{MAH}}(\text{Log} V_{m,h}) \approx 0.035$ for a $\sim 10^{12} M_\odot h^{-1}$ halo according to cosmological numerical simulations (Avila-Reese et al. 1999,2005). According to the FA-R models, the average scatter in the baryonic TFR is $\sigma_{\text{intr}}(\text{Log} V_m) \approx 0.053$ ($f_{\text{gal}} = 0.05 = \text{const.}$). This value is a lower limit under the assumptions made. It could be smaller if the distribution of λ is narrower than the one in the CDM halos. This could happen if, for example, disk galaxies form only in a subset of CDM halos, biased to have λ distribution narrower than the overall sample (e.g., D’Onghia & Navarro 2007; Dutton et al. 2007; Gnedin et al. 2007), or if the baryon spin parameter becomes smaller due to angular momentum transport processes; then the galaxies formed from the low end of the halo λ distribution would no longer be a disk type.

C.2. The R_{bar} - M_{bar} relation

According to the models of disk galaxy formation discussed above, for a given halo radius R_h , the typical size of the disk, for instance its scale length R_{bar} , is mainly proportional to $\lambda g(c) R_h$, where $g(c)$ is a function that depends weakly on the NFW halo concentration parameter c (Mo et al. 1998), given on its own by the halo MAH. Recall that detailed angular momentum conservation was assumed. The weak anti-correlation of c with M_h introduces a very weak correlation in R_{bar} with M_{bar} . Therefore, if the model parameters λ and f_{gal} ($\equiv M_{\text{bar}} / M_h$) do not depend on the mass, then the slope of the R_{bar} - M_{bar} correlation is expected to be only slightly steeper than the slope of the R_h - M_h correlation, which is ~ 0.33 (Appendix B). However, the correlation is predicted to be highly scattered, with a systematic shift in the normalization due to λ (recall that R_{bar} is directly proportional to λ while M_{bar} , in principle, is independent of λ), and also due to f_{gal} and c . The first two parameters determine the surface density of the disk; therefore, in the R_{bar} - M_{bar} diagram, the scatter should be strongly correlated with the surface density, e.g. $\Sigma_{\text{bar},0}$. Note that a dependence of λ or f_{gal} on mass would imply a change in the slope of the R_{bar} - M_{bar} correlation. For example, if λ anti-correlates with mass, then this slope will be shallower than that of the initial R_h - M_h correlation, but if f_{gal} anti-correlates with mass, then the slope will be steeper.

C.3. The V_m - R_{bar} relation

In the context of the simple models discussed in this appendix, we have $V_m \propto G(\lambda, f_{\text{gal}}) V_{m,h}$ and $R_{\text{bar}} \propto \lambda g(c) R_h$. Thus, if for the Λ CDM halos $V_{m,h} \propto R_h$, then one obtains that $V_m \propto (G[\lambda, f_{\text{gal}}] / \lambda g[c]) R_{\text{bar}}$. As mentioned above, $g(c)$ correlates very weakly with mass, and hence with radius. Then, if λ and f_{gal} are independent of mass, the expected V_m - R_{bar} correlation should be slightly shallower than the cosmological one. On the other hand, if f_{gal} correlates (anti-correlates) with mass, then the slope becomes steeper (shallower). The scatter around the V_m - R_{bar} correlation is expected to be the largest one of the three scaling relations. Galaxies are scattered in the V_m - R_{bar} diagram by their associated values of λ , f_{gal} and c . Differences in each of these val-

ues spread the galaxies in a divergent way in both axes. Therefore, the scatter of the V_m - R_{bar} relation is expected to correlate significantly with both $\Sigma_{\text{bar},0}$ and galaxy color. Recall that in the R_{bar} - M_{bar} diagram, galaxies are scattered by λ and c only along the R_{bar} axis. In the V_m - M_{bar} diagram the spread produced by these param-

eters is also only along one axis (V_m), but furthermore, the spread produced by f_{gal} in both axes is in such a way that galaxies move nearly along the main relation; that is why the TFR is the least scattered among the three relations.

REFERENCES

- Akritas, M. G., & Bershady, M. A. 1996, *ApJ*, 470, 706
 Andersen, D. R., Bershady, M. A., Sparke, L. S., Gallagher, J. S., III, & Wilcots, E. M. 2001, *ApJ*, 551, L131
 Avila-Reese, V. 2007, *Ap&SS Proc.*, "Stellar and Galactic connections between particle physics and astrophysics", Eds. A Carramiñana (Berlin: Springer), 115-164
 Avila-Reese, V., Firmani, C. 2000, *RevMexAA*, 36, 23
 Avila-Reese, V., Firmani, C., & Hernández, X. 1998, *ApJ*, 505, 37
 Avila-Reese, V., Firmani C. & Zavala, J., 2002, *ASP Conference Series*, v. 282, 137
 Avila-Reese, V., Firmani, C., Klypin, A., Kravtsov, A. 1999, *MNRAS*, 309, 507
 Avila-Reese, V., Colín, P., Gottlöber, S., Firmani, C., & Maulbetsch, C. 2005, *ApJ*, 634, 51
 Barton, E. J., Arnold, J. A., Zentner, A. R., Bullock, J. S., & Wechsler, R. H. 2007, *ApJ*, 671, 1538
 Baugh, C. M. 2006, *Reports of Progress in Physics*, 69, 3101
 Begum, A., Chengalur, J. N., Karachentsev, I. D., & Sharina, M. E. 2008, *MNRAS*, 386, 138
 Bell, E. F., & de Jong, R. S. 2001, *ApJ*, 550, 212
 Bell, E., Barnaby, D., Bower, R.G., de Jong, R.S., Harper, Jr, D.A., Hereld, M., Loewenstein, R.F. & Nauser, B.J., 2000, *MNRAS*, 312, 470
 Bell, E. F., McIntosh, D. H., Katz, N., & Weinberg, M. D. 2003a, *ApJS*, 149, 289
 Bell, E. et al. 2003b, *ApJ*, 585, L117
 Berta, Z., Jimenez, R., Heavens, A. F., & Panter, B. 2008, *ArXiv e-prints*, 802, arXiv:0802.1934
 Blanton, M. R., Geha, M., & West, A. A. 2007, *ArXiv e-prints*, 707, arXiv:0707.3813
 Bower, R. G., Benson, A. J., Malbon, R., Helly, J. C., Frenk, C. S., Baugh, C. M., Cole, S., & Lacey, C. G. 2006, *MNRAS*, 370, 645
 Bruzual, A.G., 1983, *ApJ*, 273, 105
 Bullock, J. S., Kolatt, T. S., Sigad, Y., Somerville, R. S., Kravtsov, A. V., Klypin, A. A., Primack, J. R., & Dekel, A. 2001a, *MNRAS*, 321, 559
 Bullock, J.S., Dekel, A., Kolatt, T.S., Kravtsov, A.V., Klypin, A.A., Porciani, C., & Primack, J.R., 2001b, *ApJ*, 555, 240
 Casertano, S., & van Gorkom, J.H. 1991, *AJ*, 101, 1231
 Catinella, B., Haynes, M. P., & Giovanelli, R. 2007, *AJ*, 134, 334
 Cervantes-Sodi, B., Hernandez, X., Park, Ch., & Kim, J. 2007, *MNRAS*, 388, 863
 Cimatti, A., Daddi, E., & Renzini, A. 2006, *A&A*, 453, L29
 Courteau, S., & Rix, H.-W. 1999, *ApJ*, 513, 561
 Courteau, S., MacArthur, L. A., Dekel, A., van den Bosch, F., McIntosh, D. H., & Dale, D. 2003, arXiv:astro-ph/0310440
 Courteau, S., Dutton, A. A., van den Bosch, F., MacArthur, L. A., Dekel, A., McIntosh, D. H., & Dale, D. A. 2007, *ApJ*, 671, 203
 Dalcanton, J.J., Spergel, D.N., & Summers, F.J. 1997, *ApJ*, 482, 659
 de Blok, W. J. G., & Bosma, A. 2002, *A&A*, 385, 816
 de Blok, W.J.G., van der Hulst, J.M. & Bothun, G.D., 1995, *MNRAS*, 274, 235
 de Blok, W.J.G., McGaugh, S.S. & van der Hulst, J.M., 1996, *MNRAS*, 283, 18
 de Jong, R.S. 1996a, *A&A*, 313, 45
 de Jong, R.S. 1996b, *A&A*, 313, 377
 de Jong, R.S. & van der Kruit, P.C., 1994, *A&ASS*, 106, 451
 De Rijcke, S., Zeilinger, W. W., Hau, G. K. T., Prugniel, P., & Dejonghe, H. 2007, *ApJ*, 659, 1172
 D'Onghia, E., & Navarro, J. F. 2007, *MNRAS*, 380, L58
 Dutton, A. A., van den Bosch, F. C., Courteau, S., & Dekel, A. 2005, *ArXiv Astrophysics e-prints*, arXiv:astro-ph/0501256
 Dutton, A. A., van den Bosch, F. C., Dekel, A., & Courteau, S. 2007, *ApJ*, 654, 27
 Eisenstein, D. J., & Loeb, A. 1996, *ApJ*, 459, 432
 Firmani, C., & Avila-Reese, V. 2000, *MNRAS*, 315, 457 (FA-R)
 Feigelson, E. D., & Babu, G. J. 1992, *ApJ*, 397, 55
 Franx, M., & de Zeeuw, T. 1992, *ApJ*, 392, L47
 Freeman, K. C. 1970, *ApJ*, 160, 811
 Gerritsen, J. P. E., & de Blok, W. J. G. 1999, *A&A*, 342, 655
 Giovanelli, R., et al. 2005, *AJ*, 130, 2598
 Giovanelli, R., Haynes, M. P., Herter, T., Vogt, N. P., da Costa, L. N., Freudling, W., Salzer, J. J., & Wegner, G. 1997, *AJ*, 113, 53
 Gnedin, O. Y., Kravtsov, A. V., Klypin, A. A., & Nagai, D. 2004, *ApJ*, 616, 16
 Gnedin, O. Y., Weinberg, D. H., Pizagno, J., Prada, F., & Rix, H.-W. 2007, *ApJ*, 671, 1115
 Graham, A. W. 2002, *MNRAS*, 334, 721
 Graham, A. W., & Worley, C. C. 2008, *MNRAS*, 752, in press
 Gurovich, S., McGaugh, S. S., Freeman, K. C., Jerjen, H., Staveley-Smith, L., & De Blok, W. J. G. 2004, *Publ. of the Astr. Soc. of Australia*, 21, 412
 Han, M. 1991, Ph.D. Thesis, California Inst. of Tech., Pasadena.
 Han, J., Deng, Z., Zou, Z., Wu, X.-B., & Jing, Y. 2001, *PASJ*, 53, 853
 Hernandez, X., Park, C., Cervantes-Sodi, B., & Choi, Y.-Y. 2007, *MNRAS*, 375, 163
 Hoekstra, H., Hsieh, B. C., Yee, H. K. C., Lin, H., & Gladders, M. D. 2005, *ApJ*, 635, 73
 Isobe, T., Feigelson, E. D., Akritas, M. G., & Babu, G. J. 1990, *ApJ*, 364, 104
 Jimenez, R., Verde, L., & Oh, S. P. 2003, *MNRAS*, 339, 243
 Kannappan, S. J., Fabricant, D. G., & Franx, M. 2002, *AJ*, 123, 2358
 Koda, J., Sofue, Y., & Wada, K. 2000, *ApJ*, 531, L17
 Kereš, D., Katz, N., Weinberg, D. H., & Davé, R. 2005, *MNRAS*, 363, 2
 Kodaira, K. 1989, *ApJ*, 342, 122
 MacArthur, L. A., Courteau, S., & Holtzman, J. A. 2003, *ApJ*, 582, 689
 McGaugh, S. S. 2005, *ApJ*, 632, 859
 McGaugh, S.S., de Blok, W.J.G. 1997, *ApJ*, 481, 689
 McGaugh, S. S., Schombert, J. M., Bothun, G. D., & de Blok, W. J. G. 2000, *ApJ*, 533, L99
 Mandelbaum, R., Seljak, U., Kauffmann, G., Hirata, C. M., & Brinkmann, J. 2006, *MNRAS*, 368, 715
 Mayer, L., & Moore, B. 2004, *MNRAS*, 354, 477
 Mo, H.J., Mao, S., White, S.D.M. 1998, *MNRAS*, 295, 319
 Navarro, J.F., Frenk, C.S. & White, S.D.M. 1997, *ApJ*, 490, 493
 Navarro, J. F., & Steinmetz, M. 2000, *ApJ*, 538, 477
 Paturel, G. et al. 1997, *A&ASS*, 124, 109
 Pizagno, J., et al. 2005, *ApJ*, 633, 844
 Pizagno, J., et al. 2007, *AJ*, 134, 945
 Rix, H.-W., & Zaritsky, D. 1995, *ApJ*, 447, 82
 Ryden, B. S. 2004, *ApJ*, 601, 214
 Schlegel, D. J., Finkbeiner, D. P., & Davis, M. 1998, *ApJ*, 500, 525
 Shankar, F., Lapi, A., Salucci, P., De Zotti, G., & Danese, L. 2006, *ApJ*, 643, 14
 Shen, S., Mo, H. J., & Shu, C. 2002, *MNRAS*, 331, 259
 Smith, D. R., Bernstein, G. M., Fischer, P., & Jarvis, M. 2001, *ApJ*, 551, 643
 Steinmetz, M., & Navarro, J. F. 1999, *ApJ*, 513, 555
 Stringer, M. J., & Benson, A. J. 2007, *MNRAS*, 382, 641
 Tinsley, B.M., 1981, *MNRAS*, 194, 63
 Tully, R. B., & Fisher, J. R. 1977, *A&A*, 54, 661
 Tully, R.B. & Verheijen, M.A.W. 1997, *ApJ*, 484, 145
 Tully, R. B., & Pierce, M. J. 2000, *ApJ*, 533, 744
 Tully, R.B., Pierce, M.J., Huang, J., Saunders, W., Verheijen, M.A.W. & Witchalls, P.L., 1998, *AJ*, 115, 2264
 van den Bosch, F. C., Abel, T., Croft, R. A. C., Hernquist, L., & White, S. D. M. 2002, *ApJ*, 576, 21
 Verheijen, M.A.W. 1997, Ph.D. Thesis, Groningen University
 Verheijen, M. A. W. 2001, *ApJ*, 563, 694
 Verheijen, M.A.W. & Sancisi, R., 2001, *A&A*, 370, 765
 Willick, J. A. 1999, *ApJ*, 516, 4
 Willick, J. A., Courteau, S., Faber, S. M., Burstein, D., Dekel, A., & Strauss, M. A. 1997, *ApJS*, 109, 333
 Young, J.S. & Knezek, P.M., 1989, *ApJ*, 347L, 55
 Zavala, J. 2003, B.Sc. Thesis, Universidad Nacional Autónoma de México
 Zavala, J., Avila-Reese, V., Hernández-Toledo, H., & Firmani, C. 2003, *A&A*, 412, 633 (ZAHF)